The histone chaperone CAF-1 prevents Rad52-mediated instability of the budding yeast ribosomal DNA during replication-coupled DNA double-strand break repair

Hajime Futami[1,2], Tsugumi Yamaji[4], Yuko Katayama[4], Nanase Arata[4], Takehiko Kobayashi[1,2,3]*, and Mariko Sasaki[1,4,5]*

[1]Laboratory of Genome Regeneration, Institute for Quantitative Biosciences (IQB), The University of Tokyo, 1-1-1 Yayoi, Bunkyo-ku, Tokyo 113-0032, Japan

[2]Department of Biological Sciences, Graduate School of Science, University of Tokyo, 7-3-1 Hongo, Bunkyo-ku, Tokyo 113-0033, Japan

[3]Collaborative Research Institute for Innovative Microbiology, The University of Tokyo, 1-1-1 Yayoi, Bunkyo-ku, Tokyo 113-0032, Japan

[4]Laboratory of Gene Quantity Biology, Center for Frontier Research, National Institute of Genetics, 1111 Yata, Mishima, Shizuoka 411-8540, Japan

[5]The Graduate University for Advanced Studies, SOKENDAI, 1111 Yata, Mishima, Shizuoka 411-8540, Japan

To whom correspondence should be addressed. Tel: +81 55 981 6817; Email: m_sasaki@nig.ac.jp

ABSTRACT

DNA replication-coupled chromatin assembly is crucial to maintain genome integrity. Here, we demonstrate that absence of the budding yeast histone chaperone CAF-1 induces chromosomal ribosomal RNA gene (rDNA) copy number changes as well as the production of extrachromosomal rDNA circles in a manner dependent on Fob1 that causes replication fork arrest in the rDNA, the homologous recombination protein Rad52, and its interaction with Proliferating Cell Nuclear Antigen. CAF-1 deficiency enhances transcription from the regulatory promoter E-pro, contributing to rDNA instability, but it also stabilizes the rDNA independently through its regulation of E-pro. Absence of CAF-1 induces end resection of DNA double-strand breaks (DSBs) formed at arrested replication forks, which are repaired in a manner dependent on the Mre11-Rad50-Xrs2 complex. CAF-1 deficiency causes partial defects in lagging strand synthesis coupled to nucleosome spacing in the rDNA. Our findings suggest that CAF-1 suppresses Rad52-mediated rDNA instability during repair of replication-coupled DSBs.

43 **INTRODUCTION**

44 DNA copy number changes are introduced by deletion and/or amplification of DNA segments
45 on chromosomes or via extrachromosomal circular DNAs derived from chromosomes. These
46 changes can alter gene expression levels, compromise cellular integrity, and drive
47 tumorigenesis and numerous other diseases [reviewed by (1-5)]. Thus, understanding the
48 molecular mechanisms by which chromosomal and extrachromosomal DNA copy number
49 changes occur is important.

50 The budding yeast genome contains approximately 150 rDNA copies, which are
51 tandemly repeated at a single locus on chr XII (Fig. 1A). Each copy contains 35S and 5S rRNA
52 transcription units, which are separated by intergenic spacers that contain an origin of DNA
53 replication, a cohesin-associated region (CAR), a replication fork barrier (RFB) sequence and
54 a bidirectional RNA polymerase II (RNAP II) promoter, E-pro, which synthesizes noncoding
55 RNA. Once DNA replication is initiated, the DNA replication fork progressing opposite to the
56 35S rDNA is arrested by the Fob1 protein bound to the RFB site (Fig. 1A) (6-8). The arrested
57 forks are then broken, leading to the formation of a single-ended DSB (9-11). Cells have the
58 mechanisms to maintain their rDNA copy number during DSB repair, and when these
59 mechanisms are deficient, cells undergo changes in chromosomal rDNA copy number and
60 produce extrachromosomal rDNA circles (ERCs) (Fig. 1A) (12).

61 Homologous recombination (HR) is important for repairing double-ended DSBs
62 formed independently of DNA replication, such as those introduced by endonucleases in the
63 G2/M phase of the mitotic cell cycle and meiotic DSBs [reviewed by (13,14)]. To repair DSBs
64 by HR, 5'-ended strands of the DSB ends are degraded by a process called DSB end resection
65 [reviewed in (15)]. Resected DSBs are subsequently repaired using a homologous sequence on
66 the sister chromatid as a template for Rad52-dependent recombination reactions, which
67 properly restore the original sequence at the DSB site. However, when DSBs are formed in
68 repetitive regions, HR can use a homologous template located at a misaligned position on the
69 sister chromatid or elsewhere in the genome, resulting in chromosome rearrangements
70 [reviewed by (4)].

71 Cells may use distinct mechanisms to repair DSBs that are formed in the context of
72 DNA replication forks (16). We previously demonstrated that DSB end resection is normally
73 limited for single-ended DSBs formed in the context of arrested replication forks at the rDNA
74 RFB, and these DSBs can be repaired without an essential HR factor, Rad52 (17). We have
75 identified two factors involved in suppression of DSB end resection. First, when cells lack the
76 replisome component Ctf4, DSB end resection is induced, DSB repair requires the MRX
77 complex and Rad52, and subsequent HR-dependent DSB repair results in rDNA
78 hyperamplification (17). The dependency on the MRX complex and HR proteins for DSB repair
79 seen when Ctf4 is absent is similar to the genetic requirements for repair of replication-coupled
80 DSBs introduced by nickases or endonucleases (16,18-22). Secondly, the histone deacetylase
81 Sir2 represses transcription from E-pro (Fig. 1A). When Sir2 is absent, transcription from E-
82 pro is activated, inducing DSB end resection (23). During subsequent DSB repair, HR-mediated
83 reactions are responsible for inducing chromosomal rDNA copy number changes as well as
84 ERC production, but unlike when Ctf4 is absent, cells lacking Sir2 require the MRX complex
85 but not Rad52 to complete DSB repair (23).

86 Cohesin complexes that keep sister chromatids in close proximity are recruited to the
87 CAR and RFB regions (Fig. 1A) (10,23-25) and are suggested to facilitate the use of the rDNA
88 copy at an aligned position for DSB repair (10,24). The absence of Sir2 and subsequent
89 transcriptional activation lead to the inhibition of cohesin associations with CAR and RFB and
90 rDNA instability (10,23,24). Therefore, the repression of transcription from E-pro is important
91 for maintaining rDNA stability not only by suppressing DSB end resection and subsequent HR-
92 mediated DSB repair but also by ensuring cohesin binding to rDNA (Fig. 1A).

93 Eukaryotic organisms must faithfully replicate not only their genetic information but
94 also their chromatin states to maintain genome integrity and epigenetic information. During
95 DNA replication, nucleosomes are disassembled to allow the progression of DNA replication
96 forks [reviewed by (26,27)]. Then, the parental histones are recycled and deposited onto the
97 newly replicated DNA. In addition, newly synthesized histones are deposited onto DNA *de*
98 *novo* by histone chaperones. The histone chaperone Asf1 first binds to the newly synthesized

99 histones H3-H4 and presents them to the Rtt109 acetyltransferase for acetylation at histone
100 H3K56 (28-30). Acetylated H3-H4 is then transferred to other histone chaperones such as CAF-
101 1 and Rtt106. CAF-1, which consists of Cac1, Cac2 and Cac3 in budding yeast, is recruited to
102 the replisome through its interaction with Proliferating Cell Nuclear Antigen (PCNA) and
103 deposits $(H3\text{-}H4)_2$ tetramers onto the newly synthesized DNA (31-33). These replication-
104 coupled nucleosome assembly factors play important roles in response to DNA damage but the
105 degree to which each factor contributes to different DNA damage repair pathways differs,
106 depending on the source and context of DNA damage (21,34-38). During DNA replication *in*
107 *vivo*, Okazaki fragment synthesis on the lagging strand is interlinked with the chromatin
108 assembly: Okazaki fragments show a size distribution similar to that of the nucleosome repeat,
109 and Okazaki fragment termini are located near nucleosome midpoints (39). The analysis of bulk
110 DNA synthesized during DNA replication demonstrates that CAF-1 facilitates the generation
111 of properly sized Okazaki fragments by mediating nucleosome deposition behind replication
112 forks (39-41).

113 Previous studies demonstrate that the CAF-1 complex is required for restricting HR-
114 dependent rDNA copy number loss during DSB repair in *Arabidopsis thaliana* (42-44). Here,
115 we showed that absence of the budding yeast histone chaperone CAF-1 induces not only loss
116 but also gain of chromosomal rDNA copies as well as the production of ERCs in a manner
117 dependent on Fob1 and Rad52. CAF-1 deficiency led to derepression of transcription from E-
118 pro. This transcriptional activation induced rDNA instability in the *caf-1* mutants, but other
119 defects also contributed to this phenotype. Absence of CAF-1 enhanced end resection of
120 replication-coupled DSBs at the RFB, and DSB repair and subsequent ERC production depend
121 on the MRX complex. Mutations that compromise the interaction of CAF-1 with PCNA led to
122 rDNA instability, indicating that CAF-1's function at the replication forks is important for the
123 maintenance of rDNA stability. Furthermore, CAF-1 deficiency led to a reduction in
124 nucleosome-sized Okazaki fragments in the rDNA. Taken together, these findings suggest that
125 CAF-1 is important for suppressing Rad52-dependent rDNA instability during repair of DSBs
126 formed in the context of arrested replication forks in the rDNA.

127

128 **Materials and Methods**

129 **Yeast Strains and Culture Methods**

130 Yeast strains used in this study are derivatives of W303 (*MATa ade2-1 ura3-1 his3-11, 15 trp1-*
131 *1 leu2-3,112 can1-100*) and are listed in Table S1. Haploid strains lacking genes of interest were
132 constructed by standard one-step gene replacement methods, followed by confirmation of
133 genotypes by PCR. Alternatively, diploids heterozygous for gene deletions of interest were
134 constructed, subjected to sporulation, and haploid clones were isolated by tetrad dissection.
135 Strains carrying plasmids were constructed by standard transformation methods. Yeast cells
136 were grown in YPD media (10 g/L yeast extract, 20 g/L peptone, and 20 g/L glucose). For Fig.
137 5, cells carrying plasmids were selected in SC-Trp media [6.7 g/L yeast nitrogen base without
138 amino acids (BD, 291940), 1.92 g/L yeast synthetic drop-out medium supplements without
139 tryptophan (Sigma, Y1876), 20 g/L glucose]. Agar plates were prepared similarly, with agar
140 added at 20 g/L.

141 For PFGE and ERC analyses, five mL of appropriate liquid media was inoculated with
142 cells and grown overnight to saturation at 30°C. Cultures were collected (5×10^7 cells/plug),
143 washed twice with 50 mM EDTA (pH 7.5), and cell pellets were stored at -20°C. For RNA
144 preparation, overnight cultures were diluted in 15 mL of YPAD medium (YPD containing 40
145 μg/mL adenine sulfate) to $OD_{600} = 0.2$ and grown until $OD_{600} = 0.8$. Cultures equivalent to ~1–
146 2×10^8 cells were collected, washed twice with ice-cold water, snap-frozen in liquid nitrogen,
147 and stored at -80°C. For protein extracts, overnight cultures were diluted in 15 mL to OD_{600} =
148 0.2 and grown until $OD_{600} = 0.8$. Cultures equivalent to ~0.5–1 × 10^8 cells were collected,
149 washed twice with ice-cold water, and stored at -80°C. For chromatin immunoprecipitation,
150 overnight cultures of MSY426, HFY106, and HFY122 were diluted in 100 mL of YPD medium
151 to an $OD_{600} = 0.2$ and grown until $OD_{600} = 0.8$. Cells were immediately subjected to crosslinking
152 as described below. Gal-pro WT/*cac1*Δ/*sir2*Δ strains (HF70, 73, 76) were first grown in 5 mL
153 YPD media overnight at 30°C. Cells were inoculated at ~4–5 × 10^4 cells/mL into 15 mL of YP
154 media containing 20% raffinose and grown for >24 hrs at 30°C. Cells were then inoculated at

155 2×10^6 cells/mL into two sets each of 7 mL of YP media containing either 20% raffinose or
156 20% galactose (one culture for RNA preparation and the other for agarose plug preparation).
157 To prepare RNA preparation, cultures were grown until $OD_{600} = 0.8$, collected, washed twice
158 with ice-cold water, snap-frozen in liquid nitrogen, and stored at -80°C.

159 For DSB analyses, time course experiments were performed with MSY360, 937, 1231
160 1261, and 1262, as described previously (17,45). *GAL-FOB1* strains were grown overnight in
161 YPD media at 30°C. Cells were inoculated into ~200 mL of YP media supplemented with 40
162 μg/mL adenine sulfate, 2% raffinose, and one drop of antifoam 204 (Sigma) at a density to
163 reach ~1×10^7 cells/mL the following morning and grown overnight at 23°C. To arrest cells in
164 G1 phase, α-factor (synthesized by BEX Co. Ltd. [Tokyo, Japan]) was added to cultures at a
165 final concentration of 20 nM. Cells were incubated at 23°C for 3–4 hrs until >80% of the cells
166 were arrested in G1. Then, 20% galactose was added at a final concentration of 2% to induce
167 *FOB1* expression and the cultures were further incubated for 30 min at 23°C. Cells were
168 collected by centrifugation for 5 min at 4°C at 4,500 × *g* and washed twice with YP medium
169 containing 40 μg/mL adenine sulfate and 2% galactose. Cell pellets were resuspended at ~$1 \times$
170 10^7 cells/mL in fresh YP medium containing 40 μg/mL adenine sulfate, 2% galactose, 0.075
171 mg/mL pronase E (Sigma), and one drop of antifoam 204 (Sigma), then incubated at 23°C. At
172 various time points, 10 mL culture aliquots equivalent to 1×10^8 cells were collected,
173 immediately treated with 1/100 volume of 10% sodium azide, collected, washed twice with 50
174 mM EDTA pH 7.5, and stored at -20°C. Additional 1 mL culture aliquots were collected for
175 flow cytometry analysis.

176 For analysis of Okazaki fragments, MSY613, which was derived from yIW310 that is
177 a kind gift of Iestyn Whitehouse, MSY1599, MSY1604, MSY1605 were grown overnight in
178 YPD media at 30°C. Overnight cultures were diluted in 200 mL of YPD medium to OD_{600} =
179 0.1 and grown to $OD_{600} = 0.4$. Each culture was split into two flasks. Doxycycline (100 mg/mL)
180 dissolved in DMSO was added to one culture at a final concentration of 40 μg/mL, while an

181 equal volume of DMSO was added to the other culture. After 2.5 hr incubation at 30°C, cells
182 were collected and washed twice with 50 mM EDTA (pH 8.0), and stored at -20°C.
183
184 **Plasmid construction**
185 Plasmids carrying *POL30* (pBL230-0) and mutant alleles *pol30-6* (pBL230-6), *pol30-8*
186 (pBL230-8), and *pol30-79* (pBL230-79) were kind gifts from Peter Burgers (46,47). As these
187 plasmids carry *TRP1* as a selection marker, cells transformed by these plasmids were selected
188 in SC-trp media. YCp22-CAC1 plasmid was constructed by Gibson assembly as follows. The
189 genomic region containing the *CAC1* open reading frame with a few hundred bp upstream and
190 downstream regions were amplified by PCR from the *S. cerevisiae* WT strain of the W303
191 background, using primers 5'-TGCATGCCTGCAGAGATCTACATCGTTAAACCAAAAG
192 and 5'-GAGCTCGGTACCTTGCATGCGAGAAGTGCTG. Linearized YCplac22 was
193 generated by PCR from YCplac22 with primers 5'-
194 GATGTAGATCTCTGCAGGCATGCAAGCTTG and 5'-
195 TCTCGCATGCAAGGTACCGAGCTCGAATTC. These PCR fragments had short homology
196 at each end and were fused using Gibson Assembly (New England Biolabs) according to the
197 manufacturer's instructions. YCp22-cac1-20 plasmid carrying the *cac1-20* mutation was
198 constructed using the PrimeSTAR Mutagenesis Basal Kit (TaKaRa) with YCp22-CAC1 as a
199 template and primers 5'-GTAACGCCGGTAAAAAACTAAGCGATTCTAATA and 5'-
200 TTTTACCGGCGTTACCAATACGGGATTGTGCTC, according to the manufacturer's
201 instructions.
202 YCp22-CAC1-9myc and YCp22-cac1-20-9myc plasmids were constructed by
203 inserting the sequence that encodes nine consecutive myc epitope tag prior to the stop codon of
204 *CAC1* and *cac1-20* as follows. The 9myc sequence was amplified by PCR using pYM19 (48)
205 and primers 5'-CCAACCCCGTCTTTGCGTACGCTGCAGGTCGAC and 5'-
206 GATCCGTTCAAGTTAGCTAGTGGATCCGTTC. YCp22-CAC1 and YCp22-cac1-20 were
207 linearized with the primers 5'-CAAAGACGGGGTTGGC and 5'-
208 TAACTTGAACGGATCTTTAGTATATAGAA. These PCR fragments had short homology at

209 each end and were fused using In-Fusion Snap Assembly Master Mix (TaKaRa Bio Inc., Japan),
210 according to the manufacturer's instructions. Plasmid DNA was sequenced to confirm that it
211 had the proper mutation or insertion.
212
213 **Genomic DNA preparation**
214 For PFGE, ERC, and DSB gel analyses, genomic DNA was prepared in low melting
215 temperature agarose plugs as described previously (17,45). Briefly, collected cells were
216 resuspended in 50 mM EDTA pH 7.5 (33 μL per 5×10^7 cells) and incubated at 42°C. For each
217 plug, 33 μL cell suspension was mixed with 66 μL of solution 1 (0.83% low-melting-point
218 agarose SeaPlaque GTG (Lonza), 170 mM sorbitol, 17 mM sodium citrate, 10 mM EDTA (pH
219 7.5), 0.85% β-mercaptoethanol, and 0.17 mg/mL Zymolyase 100 T (Nacalai)), poured into a
220 plug mold (Bio-Rad) and placed at 4°C until the agarose was solidified. Plugs were transferred
221 to a 2 mL tube containing solution 2 (450 mM EDTA pH 7.5, 10 mM Tris-HCl pH 7.5, 7.5% β-
222 mercaptoethanol and 10 μg/mL RNaseA (Macherey-Nagel)) and incubated for 1–1.25 hrs at
223 37°C. Plugs were then incubated overnight at 50°C in solution 3 (250 mM EDTA pH 7.5, 10
224 mM Tris-HCl pH 7.5, 1% sodium dodecyl sulfate (SDS) and 1 mg/mL proteinase K (Nacalai)).
225 Plugs were washed four times with 50 mM EDTA (pH 7.5) and stored at 4°C in 50 mM EDTA
226 (pH 7.5).
227 For analysis of Okazaki fragments, genomic DNA was isolated as described previously
228 (39), with slight modifications. Briefly, cells were washed twice with lysis buffer (50 mM Tris-
229 HCl [pH 8.0], 50 mM EDTA [pH 8.0], 100 mM NaCl, and 1.5% SDS). Cells were then
230 resuspended in 900 μL of SCE solution (1 M sorbitol, 0.1 M sodium citrate, 0.06 M EDTA [pH
231 7.5]) supplemented with 35 μL of β-mercaptoethanol and 100 μL of 50 mg/mL Zymolyase and
232 mixed by vortexing. After incubating the cell suspension for 3 min at room temperature,
233 spheroplasts were collected by centrifugation for 5 min at 4,500 × *g* and rinsed with 1 mL of
234 SCE and collected by centrifugation for 5 min at 4,500 × *g*. Spheroplasts were resuspended in
235 500 μL of lysis buffer (50 mM EDTA (pH 8.0), 50 mM Tris-HCl (pH 8.0), 0.5% sodium dodecyl

236 sulfate, and 200 μg/mL proteinase K) and incubated for 2 hrs at 42°C. Proteins were precipitated
237 by adding 200 μL of 5 M potassium acetate, incubating for 5 min on ice, and centrifuging at
238 15,000 rpm for 15 min at 4°C. DNA in the supernatant was precipitated with isopropanol and
239 resuspended in 250 μL of STE (10 mM Tris-HCl [pH 8.0], 1 mM EDTA [pH 8.0], 100 mM
240 NaCl containing 80 μg/mL RNaseA [Macherey-Nagel]). RNA was digested by incubation for
241 1 hr at 37°C. DNA was ethanol precipitated, suspended in 50 μL of TE, and quantified using a
242 Qubit Fluorometer.
243
244 **PFGE**
245 PFGE was performed as described previously (17,45). Briefly, one-third of a plug was placed
246 on a tooth of the comb, alongside a piece of *Hansenula wingei* chromosomal DNA markers
247 (Bio-Rad). The comb was placed in a gel tray, and 1.0% agarose solution (Pulsed Field Certified
248 Agarose, Bio-Rad) in 0.5× TBE (44.5 mM Tris base, 44.5 mM boric acid and 1 mM EDTA pH
249 8.0) was poured. PFGE was performed on a Bio-Rad CHEF Mapper XA Chiller System in 2.2
250 L of 0.5× TBE under the following conditions: 3.0 V/cm for 68 hrs at 14°C, 120° included angle,
251 with initial and final switch times of 300 s and 900 s, respectively. After electrophoresis, DNA
252 was stained with 0.5 μg/mL ethidium bromide (EtBr) for 30 min, washed with dH_2O for 30 min,
253 and then photographed.
254
255 **Southern blotting**
256 ***Agarose gel electrophoresis***
257 ***ERC assay.*** The ERC assay was performed as described previously (23,45). Half of the
258 agarose plug was placed on a tooth of the comb. After setting the comb in the gel tray (15 × 25
259 cm), 300 mL of 0.4% agarose (SeaKem LE Agarose, Lonza) in 1× TAE (40 mM Tris base, 20
260 mM acetic acid, and 1 mM EDTA pH 8.0) was poured into the tray and allowed to solidify.
261 Lambda HindIII DNA marker (600 ng) was loaded in an empty lane. Electrophoresis was
262 performed on a Sub-cell GT electrophoresis system (Bio-Rad) in 1.45 L of 1× TAE at 1.0 V/cm

263 for ~20–48 hrs at 4°C with buffer circulation. The buffer was changed every ~24 hrs. DNA was
264 stained with 0.5 μg/mL ethidium bromide (EtBr) for 30 min and then photographed.

265 ***DSB assay.*** The DSB assay was performed as described previously (17,45). One-third
266 of an agarose plug was cut and placed in a 2 mL tube. The plug was equilibrated four times in
267 1 mL of 1× TE (10 mM Tris base, pH 7.5 and 1 mM EDTA, pH 8.0) by rotating the tube for 15
268 min at room temperature. The plug was then equilibrated twice in 1 mL of 1× NEBuffer 3.1
269 (New England Biolabs) by rotating the tube for 30 min at room temperature. After discarding
270 the buffer, the plug was incubated in 160 μL of 1× NEBuffer 3.1 buffer containing 160 units of
271 Bgl II (New England Biolabs) overnight at 37°C. The plug was placed on a tooth of the comb
272 which was set into the gel tray (15 × 25 cm), into which 0.7% agarose solution in 1× TBE was
273 poured; after the gel was solidify, 600 ng of lambda BstEII DNA markers were loaded in an
274 empty lane. Electrophoresis was performed on a Sub-cell GT electrophoresis system (Bio-Rad)
275 in 1.45 L of 1× TBE at 2.0 V/cm for 22 hrs at room temperature with buffer circulation. After
276 electrophoresis, DNA was stained with 0.5 μg/mL EtBr for 30 min and then photographed.

277 ***Okazaki fragment assay.*** DNA samples were prepared in 20 μL containing 500 ng of
278 genomic DNA, 2 μL of 10× alkaline buffer (0.5 M NaOH, 10 mM EDTA [pH 8.0]), 2 μL of
279 0.1% bromophenol blue, and 1 μL of 50% glycerol, which were heat-denatured for 5 min at
280 70°C, followed by rapid chilling on ice. A total of 500 ng of 100 bp DNA ladder was similarly
281 denatured. The agarose solution was prepared by dissolving 2.5 g of Seakem LE agarose
282 (Lonza) in 225 mL of Milli-Q water by microwave, followed by cooling to 50°C. Then, 25
283 mL of 10× alkaline buffer was added to the agarose solution, mixed, poured into a gel tray (15
284 × 20 cm) in a cold room, and left until the gel solidified. The comb was removed, and 1.45 L
285 of 1× alkaline buffer was added. DNA samples were loaded. The gel was run overnight for 4
286 hrs at 4°C at 80 V.

287 ***DNA transfer***

288 After agarose gel electrophoresis, DNA was transferred to Hybond-XL (GE Healthcare) by the
289 standard capillary transfer method. Alternatively, DNA was vacuum-transferred to Hybond-XL
290 (GE Healthcare) or Nytran SPC (Cytiva) using VacuGene XL (GE Healthrecare). Vacuum was

291 applied at 55 cm Hg for 30–45 min with freshly prepared 0.25 N HCl, for 20–30 min with
292 denaturation solution (0.5 N NaOH, 1.5 M NaCl), and for 1 hr 40 min–2 hrs with transfer buffer
293 (0.25 N NaOH, 1.5 M NaCl). After transfer, DNA was fixed to the membrane by soaking the
294 membrane in 300 mL of freshly prepared 0.4 N NaOH for 10 min with gentle shaking, followed
295 by rinsing the membrane with 2× SSC for 10 min. The membrane was subsequently dried and
296 stored at 4°C.

297 ***Probe preparation***

298 Probes were prepared as described previously (17,45). Double-stranded DNA fragments were
299 amplified by PCR. Probe 1 used for ERC and Okazaki fragment analyses was amplified with
300 the primers 5'-CATTTCCTATAGTTAACAGGACATGCC and 5'-
301 AATTCGCACTATCCAGCTGCACTC, and probe 4 used for DSB analysis was amplified with
302 the primers 5'-ACGAACGACAAGCCTACTCG and 5'-AAAAGGTGCGGAAATGGCTG. A
303 portion of the PCR products was gel-purified and used as templates for a second round of PCR
304 with the same primers. The PCR products were then gel-purified. Fifty ng of purified PCR
305 products was used for random priming reactions in the presence of the radiolabeled nucleotide,
306 [α-^{32}P]-dCTP (3,000 Ci/mmol, 10 mCi/mL, Perkin Elmer), using Random Primer DNA
307 Labeling Kit (TaKaRa), according to the manufacturer's instructions. For Fig. 4G and 4I, 50 ng
308 of gel-purified PCR products were labeled with digoxigenin (DIG)-11-dUTP using DIG-High
309 Prime (Roche), according to the manufacturer's instructions. Unincorporated nucleotides were
310 removed using ProbeQuant G-50 Micro Columns (GE Healthcare). Radiolabeled probes were
311 heat-denatured for 5 min at 100°C, immediately prior to hybridization to the membrane.

312 ***Hybridization***

313 Southern hybridization was performed as described previously (17,23,45). The membrane was
314 prewetted with 0.5 M phosphate buffer pH 7.2 and prehybridized for 1 hr at 65°C with 25 mL
315 of hybridization buffer (1% bovine serum albumin, 0.5 M phosphate buffer, pH 7.2, 7% SDS,
316 1 mM EDTA pH 8.0). After discarding the buffer, the membrane was hybridized overnight at
317 65°C with 25 mL of hybridization buffer containing heat-denatured probe. The membrane was

318 washed four times for 15 min at 65°C with wash buffer (40 mM phosphate buffer pH 7.2, 1%
319 SDS, 1 mM EDTA pH 8.0) and exposed to a phosphor screen.

320 Non-radioactive hybridization in Fig. 4G and 4I was performed using DIG-High Prime
321 DNA Labeling and Detection Starter Kit II, CPD-*Star*, and DIG Wash and Block Buffer Set
322 (Roche) according to the manufacturer's instructions. Briefly, membranes were prewetted with
323 2× SSC and prehybridized for 1 hr at 42°C in DIG Easy Hyb buffer. After the buffer was
324 discarded, membranes were hybridized overnight at 42°C with DIG Easy Hyb buffer containing
325 heat-denatured probe. Membranes were washed twice for 15 min at 65°C with 2× SSC, 0.1%
326 SDS and then twice for 15 min at 65°C with 0.5× SSC, 0.1% SDS. After a 5 min wash at room
327 temperature with Washing buffer, membranes were blocked for 30 min at room temperature
328 with Blocking solution, and Blocking solution was discarded. Membranes were incubated for
329 30 min at room temperature with Anti-Digoxigenin AP diluted by 20,000 fold in Blocking
330 solution. Membranes were washed twice for 15 min with Washing solution and treated for 5
331 min with Detection buffer. CDP *Star* was added onto the membrane drop-wise, followed by
332 incubation for 5 min. Then, chemiluminescent signals were detected on Bio-Rad ChemiDoc
333 MP.

334 ***Image analysis***

335 ***ERC assay.*** Radioactive signals were detected using a Typhoon FLA 7000 or 9000 (GE
336 Healthcare). The chromosomal rDNA signal was used for normalization of the ERC signals.
337 Thus, the membranes hybridized with radioactive probes were exposed to the phosphor screen
338 for a short time and scanned before signal saturation. Then, membranes were re-exposed to a
339 phosphor screen for several days to achieve optimal signal-to-noise ratios for ERCs. For
340 detection of DIG-labeled probes, chemiluminescent signals were detected after short exposure
341 before signal saturation. Subsequently, membranes were exposed for longer time to achieve
342 optimal signal-to-noise ratio for ERCs. ERC bands and chromosomal rDNA band were
343 quantified from images after long and short exposures, respectively, using FUJIFILM Multi
344 Gauge version 2.0 software (Fujifilm) or Amersham ImageQuant TL ver. 10.2 (Cytiva). ERC
345 levels were calculated as the ratio of ERC signal intensities to chromosomal rDNA signals.

346 When the levels of ERCs were compared between samples loaded on different gels, control
347 DNA plugs were included on each gel for normalization.

348 ***DSB assay.*** Membranes were exposed to a phosphor screen for 1–4 days until signals
349 of linear molecules, but not arrested forks, DSBs, or resected DSB signals, reached saturation.
350 The frequency of DSBs and resected DSBs was determined as described previously (17,45).
351 Briefly, in each lane, signal intensities of arrested forks, DSBs, resected DSBs, and the terminal
352 fragment containing the telomere-proximal rDNA repeat and its adjacent non-rDNA fragment
353 were quantified using FUJIFILM Multi Gauge version 2.0 software (Fujifilm) or Amersham
354 ImageQuant TL ver. 10.2 (Cytiva). All signals were normalized to the terminal fragment, and
355 the value at t = 0 min was then subtracted from those at other time points. The DSB frequency
356 was calculated as the ratio of maximum DSB level to maximum arrested fork level in the same
357 time course. The frequency of DSB end resection was determined by dividing the maximum
358 level of resected DSBs by the maximum level of DSBs in the same time course.

359 ***Okazaki fragment assay.*** Membranes were exposed to a phosphor screen for several
360 days. Lane profiles of signal intensity of each lane were analyzed using ImageJ (NIH).

361

362 **Yeast RNA preparation**

363 RNA was prepared as described previously (49), with slight modifications. Collected cells were
364 resuspended in 400 μL of TES (10 mM Tris-HCl pH 7.5, 10 mM EDTA pH 7.5, 0.5% SDS) and
365 400 μL of acidic phenol by vortexing for approximately 10 s. Cells were incubated at 65°C for
366 1 hr with occasional vortexing every 15 min. Cell suspensions were then incubated for 5 min
367 on ice and centrifuged at 20,000 × *g* for 10 min at 4°C. The aqueous phase was transferred to a
368 new tube and mixed with an equal volume of acidic phenol by vortexing for 10 s. After 5 min
369 incubation on ice and centrifugation at 20,000 × *g* for 10 min at 4°C, the aqueous phase was
370 transferred to a new tube. RNA was precipitated overnight at -20°C by adding 1/10 volume of
371 3 M sodium acetate (pH 5.3) and 2.5 volumes of 100% ethanol. The precipitate was collected
372 by centrifugation at 20,000 × *g* for 10 min at 4°C and washed with 70% ethanol. RNA pellets
373 were resuspended in 30 μL of dH_2O treated with 0.1% diethylpyrocarbonate (DEPC). RNA

374 concentration was determined using a NanoDrop ND-1000 spectrophotometer (Thermo Fisher
375 Scientific). Samples were stored at -80°C.
376
377 **Northern blotting**
378 Total RNA (30 μg) was brought up to 7 μL with DEPC-treated dH_2O and mixed with 17 μL of
379 RNA sample buffer (396 μL of deionized formamide, 120 μL of 10× MOPS buffer [0.2 M
380 MOPS, 50 mM sodium acetate pH 5.2, 10 mM EDTA pH 7.5 in DEPC-treated dH_2O], and 162
381 μL of 37% formaldehyde). A total of 1.8 μg of DynaMarker RNA High Markers (BioDynamics
382 Laboratory) were brought up to 4.8 μL with DEPC-treated dH_2O and mixed with 11.2 μL of
383 RNA sample buffer. Samples were heated at 65°C for 20 min and rapidly chilled on ice. To the
384 samples, 6 μL of 6× Gel Loading Dye (B7025S, New England Biolabs) and 1.5 μL of 2.5
385 mg/mL EtBr were added. To the size markers, 4 μL of 6× Gel Loading Dye (B7025S, New
386 England Biolabs) and 1 μL of 2.5 mg/mL EtBr were added.
387 Two 1% agarose gels were prepared by dissolving 1 g of agarose in 73 mL of DEPC-
388 treated dH_2O. After cooling to 60°C, 17 mL of 37% formaldehyde and 10 mL of 10× MOPS
389 buffer were added. The solution was poured into a gel tray (13 × 12 cm) and allowed to set.
390 Agarose gel electrophoresis was performed on a Mupid EX system (Takara) in 400 mL of 1×
391 MOPS buffer at 20 V for 20 min and then at 100 V until the bromophenol blue dye migrated
392 approximately 2/3 of the gel. Gels were photographed and RNA was transferred to Hybond-N+
393 (GE Healthcare) by standard capillary transfer.
394 Strand-specific probes were prepared from double-stranded DNA fragments, amplified
395 by PCR and gel-purified. The PCR primers used for probe 2 (against IGS1-R, IGS2-R), 5'-
396 TCGCCAACCATTCCATATCT and 5'-CGATGAGGATGATAGTGTGTAAGA; for probe 3
397 (against IGS1-F) were 5'-AGGGAAATGGAGGGAAGAGA and 5'-
398 TCTTGGCTTCCTATGCTAAATCC, and for detecting *TSA1*, 5′-
399 CAAGTTCAAAAGCAAGCTCC and 5′-ACCAATCTCAAGGCTTCGTC. Strand-specific
400 probes were then prepared by linear PCR in a final volume of 20 μL containing 0.2 mM dATP,

401 0.2 mM dTTP, 0.2 mM dGTP, 50 μL [α-^{32}P]-dCTP (3,000 Ci/mmol, 10 mCi/mL, Perkin Elmer),
402 1.25 units ExTaq (TaKaRa), 1× ExTaq buffer, 50 ng of PCR product as a template, and 10 μM
403 primer (5'-AGTTCCAGAGAGGCAGCGTA for probe 2, 5'-CATTATGCTCATTGGGTTGC
404 for probe 3). PCR was initiated by a denaturation step at 94°C for 3 min, followed by 35 cycles
405 of amplification (96°C for 20 s, 51°C for 20 s, and 72°C for 30 s), and a final step at 72°C for
406 3 min. Unincorporated nucleotides were removed using ProbeQuant G-50 Micro Columns (GE
407 Healthcare). Radiolabeled probes were heat denatured by incubating for 5 min at 100°C,
408 immediately prior to hybridization to the membrane.

409 Membrane was incubated with 10 mL of ULTRAhyb Ultrasensitive Hybridization
410 Buffer (Thermo Fisher) at 42°C for 1 h. The heat-denatured probe was incubated with the
411 membrane overnight at 42°C. The membrane was rinsed twice with 2× SSC, washed for 15 min
412 at 42°C twice with wash buffer 1 (2× SSC, 0.1% SDS), and washed for 15 min at 42°C twice
413 with wash buffer 2 (0.1× SSC, 0.1% SDS). The membrane was exposed to phosphor screens
414 for several days, and radioactive signals were detected using a Typhoon FLA 7000 (GE
415 Healthcare). Probes were stripped by incubating the membrane with boiled 0.1% SDS by
416 shaking for ~30 min, rinsed with 2× SSC, and rehybridized with the *TSA1* probe that was
417 prepared as described above. Signals of IGS-F, IGS1-R, IGS2-R, and *TSA1* were quantified
418 using FUJIFILM Multi Gauge version 2.0 software (Fujifilm). The levels of IGS transcripts
419 were normalized to the *TSA1* signal.

420

421 **Preparation of protein extracts**

422 Protein extracts were prepared from yeast cells, as described previously with slight
423 modifications (49). Cells were resuspended in 500 μL of ice-cold dH_2O and 75 μL of Alkali-
424 2ME solution (1.295 N NaOH and 7.5% v/v 2-mercaptoethanol) by vortexing and incubated
425 on ice for 10 min. Cell suspensions were mixed with 75 μL of 50% w/v trichloroacetic Acid
426 by vortexing and incubated on ice for 10 min. After centrifugation at 10,000 × *g* for 5 min at
427 4°C, the supernatant was completely removed and pellets were resuspended in 75 μL of buffer
428 (800 μL of 200 mM Tris-HCl pH 8.8 and 200 μL of 5x SDS-loading buffer [250 mM Tris-

429 HCl, pH 6.8, 10% SDS, 0.1% bromophenol blue, 25% glycerol, 25% β-mercaptoethanol]).
430 Protein concentration was quantified using a Bradford assay (Bio-Rad). Protein samples were
431 stored at -20°C.
432
433 **Western blotting**
434 Protein samples (30 μg) were mixed with 1× SDS-loading buffer to a final volume of 10 μL.
435 Protein samples were heated for 5 min at 65°C, and centrifuged at 20,000 × *g* for 5 min at
436 4°C. Supernatants were loaded and separated on 5–20% pre-made Bullet PAGE Plus Precast
437 Gel (Nacalai Tesque) in 400 mL of 1x SDS-PAGE running buffer (25 mM Tris, 192 mM
438 Glycine, 0.1% SDS). Proteins were transferred to Immobilon-P PVDF membrane (Merck-
439 Millipore) in 1× transfer buffer (25 mM Tris, 192 mM glycine, 10% methanol) for 60 min at
440 100 V at 4°C using a Mini Trans-Blot cell (Bio-Rad). After transfer, the membrane was
441 blocked in 5% Skim Milk (Wako) in TBS-T (1x TBS, 0.1% Tween20) for 1 hr at room
442 temperature. The membrane was incubated overnight at 4°C with anti-myc antibody (9E10)
443 (Santa Cruz, sc-40) diluted by 1,000-fold in 1% skim milk in TBST. The membrane was
444 washed three times for 5 min with TBS-T. The membrane was further incubated with anti-
445 mouse IgG-HRP (GE Healthcare, NA931VS) diluted by 10,000-fold in 1% milk in TBST for
446 1 hr at room temperature. The membrane was washed three times for 5 min with TBS-T. The
447 membrane was incubated with ECL Prime (GE Healthcare) and chemiluminescent signal was
448 detected on Bio-Rad ChemiDoc MP. Antibodies were stripped by incubating for 30 min at
449 room temperature in Western BLoT Stripping Buffer (TaKaRa Bio). From the same
450 membrane, tubulin was detected as a loading control. The membrane was blocked in 5% Skim
451 Milk in TBS-T for 1 hr at room temperature. The membrane was incubated overnight at 4°C
452 with anti-tubulin-HRP (YL1/2) (BIO-RAD, BCA77P) diluted by 1,000-fold in 1% milk in
453 TBS-T. After the membrane was washed three times for 5 min with TBS-T, the membrane
454 was incubated with ECL Prime (GE Healthcare) and chemiluminescent signal was detected
455 on BIO-RAD ChemiDoc MP. Protein signals were quantified using Image Lab software
456 (BIO-RAD).

457

458 **Chromatin immunoprecipitation-quantitative PCR analysis**

459 Thirty-five milliliters of cultures were transferred to 50 mL conical tubes and crosslinked with
460 972 μL of 37% formaldehyde (1% final concentration) by shaking for 30 min at room
461 temperature on a reciprocal shaker at 60 r/min. The reaction was quenched with glycine (a final
462 concentration of 125 mM) by shaking for 5 min at room temperature on a reciprocal shaker at
463 60 r/min. Cells were collected by centrifugation at 2,380 × *g* for 3 min at 4°C, washed twice
464 with 20 mL of TBS (20 mM Tris, 150 mM NaCl, pH 7.4), and washed once with 5 mL of FA
465 lysis buffer (50 mM HEPES-KOH, pH 7.4; 150 mM NaCl; 1 mM EDTA, pH 8.0; 1% Triton
466 X-100; 0.1% sodium deoxycholate; 0.1% SDS). Cell pellets were resuspended in 0.5 mL of FA
467 lysis buffer, transferred to a 1.5 mL microtube, and collected by centrifugation at 2,380 × *g* for
468 1 min at 4°C.

469 Cells were resuspended in 400 μL of FA lysis buffer containing 1 mM PMSF and 1×
470 Complete EDTA-free solution, transferred to a 2 mL tube (STC-0250, Yasui Kikai), and mixed
471 with 1.5 g of 0.5 mm Zirconia/silica beads. Cells were disrupted using a Multibead Shocker
472 (Yasui Kikai) for 20 cycles of 30 sec on at 2,700 rpm and 30 sec off at 2°C. A burned 23–26-
473 G needle was used to make a few holes at the bottom of the tube, which was inserted into a 5
474 mL tube and centrifuged at 1,000 × *g* for 30 sec at 4°C. The cell lysate was transferred to a 1.5
475 mL TPX tube. Chromatin was sheared by sonication at 4°C at high power with ice on a
476 Bioruptor for three sets of 5 cycles of 30 sec on and 30 sec off. Sheared chromatin samples
477 were centrifuged at 20,380 × *g* for 15 min at 4°C and recovered with the same volume of FA
478 lysis buffer. A total of 10 μL was set aside as input DNA.

479 A total of 320 μL was transferred to a low-binding tube (Costar) and incubated with 10
480 μL of Dynabeads Protein G (Thermo Fisher) for 1 hr at 4°C, after which the precleared samples
481 were transferred to a new low-binding tube. Then, 2.1 μg of anti-Flag antibody (M2; Sigma–
482 Aldrich) was added to each tube, and the mixture was incubated for 3 hrs at 4°C. Chromatin
483 samples were incubated with an antibody and then incubated overnight at 4°C with 12 μL of

484 Dynabeads Protein G, which was preincubated with 5 mg/mL BSA solution in PBS. Beads
485 were washed twice with 0.5 mL of FA lysis buffer, twice with 0.5 mL of FA lysis buffer
486 supplemented with 360 mM NaCl, twice with 0.5 mL of ChIP wash buffer (10 mM Tris-HCl
487 (pH 8.0), 250 mM lithium chloride, 1 mM EDTA (pH 8.0), 0.5% NP-40 and 0.5% sodium
488 deoxycholate), and twice with 0.5 mL of 1× TE buffer. After the buffer was completely
489 removed, 54 μL of ChIP elution buffer (50 mM Tris-HCl (pH 8.0), 10 mM EDTA, and 1%
490 SDS) was added, and the immunoprecipitates were eluted from the beads by incubating for 15
491 min at 65°C. Fifty μL of eluate was transferred to a new tube and mixed with 150 μL of TE
492 containing 1% SDS. Ten μL of input sample was mixed with 190 μL of TE containing 1%. To
493 each sample, RNaseA was added at a final concentration of 50 μg/mL. These samples were
494 incubated overnight at 65°C for reverse crosslinking and RNA digestion. Then, proteinase K
495 was added at a final concentration of 0.75 mg/mL, and the mixture was incubated for 2 hrs at
496 50°C. DNA was purified using a QIAquick PCR Purification Kit (QIAGEN). DNA was eluted
497 with 100 μL of dH_2O.

498 qPCR was performed on a Thermal Cycler Dice Real Time System II (TaKaRa) with
499 THUNDERBIRD SYBR qPCR Mix or Next SYBR qPCR Mix (TOYOBO) according to the
500 manufacturers' instructions. One of the input samples was diluted serially to 1/20, 1/200,
501 1/2,000 and 1/20,000 dilutions, which were subsequently used to construct the standard curve.
502 All the input samples were subsequently diluted 400-fold. IP samples were diluted 10-fold.
503 qPCR was performed with all the diluted samples as well as the standard. The primers used are
504 as follows: in Fig. 3A (i) 5'-AAAATCTCGACCCTTTGGAAGA and 5'-
505 AATGAACCATCGCCAGCAC ; Fig. 3A (ii) 5'-GTGCAAAAGACAAATGGATGG and 5'-
506 GGTGCCGTAAATGCAAAACA; Fig. 3A (iii) 5'-TGCAAAGATGGGTTGAAAGAGA and
507 5'-TTTGCCGCTCTGATGGTG; Fig. 3A (iv) 5'-AACGCGGTGATTTCTTTGCT and 5'-
508 TTGCTAGCCTGCTATGGTTCA; Fig. 3B 5'-ACGAACTTAAGGCCGCAGTA and 5'-
509 CTTCGACAGGTTCCATAACG; Fig. 3C 5'-GCTGGGTCTCACGATCCATATCAG and 5'-
510 TCTTGTTTCGGTGAGTTGGACAGATC. The amount of DNA in each sample was

511 subsequently determined relative to the standard. After considering dilution factors, % input
512 was expressed for each time point of each culture as the amount of DNA in the IP relative to
513 that in the input.
514
515 **Fluorescence-activated cell sorter analysis**
516 Approximately 1 × 10^7 cells were collected at different time points during time course
517 experiments. Cells were fixed with 200 µL of 70% ethanol at -20°C overnight. Cells were
518 collected, resuspended in 200 µL of 50 mM sodium citrate at pH 7.5 containing 0.25 mg/ml
519 RNaseA (Macherey-Nagel) and incubated for 1 hr at 50°C. Then, 100 µL of 50 mM sodium
520 citrate pH 7.5 containing 1 mg/ml Proteinase K (Nacalai) was added and cells were incubated
521 for 1 hr at 50°C. 300 µL of 50 mM sodium citrate pH 7.5 containing 4 µg/ml propidium iodide
522 (Sigma) was added. Cells were sonicated and diluted with 50 mM sodium citrate pH 7.5
523 containing 4 µg/ml propidium iodide when necessary and were analyzed using a BD Accuri C6
524 Plus Flow Cytometer (BD Bioscience).
525
526 **Quantification and statistical analysis**
527 Statistical analyses were performed using GraphPad Prism, as described in Figure legends.
528
529 **RESULTS**
530 **CAF-1 suppresses HR-mediated rDNA instability in response to Fob1-dependent**
531 **replication fork arrest.**
532 To test whether Cac1, Cac2 and Cac3 function as a complex in maintaining rDNA stability, we
533 compared the degree of rDNA instability in *cac1*Δ, *cac2*Δ, and *cac3*Δ single mutants. We
534 isolated genomic DNA from these mutants, separated it by pulsed-field gel electrophoresis
535 (PFGE), and examined the size heterogeneity of chr XII carrying the rDNA array. The wild-
536 type (WT) strain showed homogeneous chr XII bands, while all single *caf-1* mutants showed
537 extremely smeared bands to the degree seen in the *sir2*Δ mutant (Fig. 1B). Consistent with our

538 previous finding (50), the absence of the subunits of budding yeast CAF-1 induced both
539 contraction and expansion of the chromosomal rDNA cluster.

540 Cells lacking any subunit of the budding yeast CAF-1 showed increased ERC
541 formation (Fig. 1C, 1D and Supplementary Fig. S1A). ERC levels in *cac1*Δ and *cac2*Δ single
542 mutants were ~3-fold greater than those in the WT strain and their levels were comparable to
543 that in the *sir2*Δ mutant (Fig. 1C, 1D). The *cac3*Δ mutant showed less severe rDNA instability
544 than *cac1*Δ and *cac2*Δ mutants did but still exhibited a ~1.7-fold increase in the ERC level,
545 compared to the WT strain (Fig. 1C, 1D). While monomeric ERCs were predominant in the
546 WT, the *caf-1* mutants produced more dimeric and multimeric ERCs (Fig. 1E). In both PFGE
547 and ERC analyses, the phenotypes of double and triple *caf-1* mutants were similar to those of
548 *cac1*Δ and *cac2*Δ single mutants (Fig. 1C–1E). Therefore, Cac1, Cac2 and Cac3 function as a
549 complex to stabilize the rDNA by suppressing chromosomal rDNA copy number changes and
550 the production of ERCs, particularly multimeric ERCs.

551 To elucidate how CAF-1 maintains rDNA stability, we examined whether rDNA
552 instability in the *cac1*Δ mutant depends on Fob1 and the HR protein Rad52. We constructed a
553 diploid strain heterozygous for *cac1*Δ, *fob1* and *rad52*Δ, isolated haploid clones by tetrad
554 dissection, and analyzed their rDNA stability by PFGE. The *cac1*Δ mutant showed smeared chr
555 XII bands, but this smearing was suppressed by an introduction of a *fob1* mutation, suggesting
556 that rDNA instability in the *cac1*Δ mutant depends on Fob1 (Fig. 1F), consistent with a previous
557 finding (50). Smearing of the chr XII bands in the *cac1*Δ mutant was also suppressed by *rad52*Δ
558 (Fig. 1F). Furthermore, ERC production in the *cac1*Δ mutant was suppressed by both *fob1* and
559 by *rad52*Δ (Fig. 1G, 1H). Similar suppression of rDNA instability by *fob1* and *rad52*Δ was
560 observed in *cac2*Δ and *cac3*Δ mutants (Supplementary Fig. S1B–S1E). Thus, CAF-1
561 suppresses Rad52-mediated rDNA instability in response to Fob1-dependent replication fork
562 arrest at the RFB.

563

564 **CAF-1 stabilizes the rDNA in a manner both dependent and independent of repression of**
565 **transcription from E-pro.**
566 CAF-1 is involved in gene silencing at telomeres and silent mating type loci, as well as in
567 silencing marker genes inserted in rDNA (33,51,52). We next examined whether CAF-1 is
568 involved in the regulation of transcription from the native noncoding RNA promoter E-pro. We
569 extracted total RNA from WT, *cac1*Δ, *cac2*Δ and *cac3*Δ mutants, separated RNA by agarose
570 gel electrophoresis under denaturing conditions, and detected transcripts from E-pro by
571 Northern blotting with strand-specific probes (Fig. 2A). The *sir2*Δ mutant, in which
572 transcription from E-pro is derepressed (24), was analyzed in parallel.
573 IGS1-R transcripts of ~300–650 nt in size were detected in the *sir2*Δ mutant, consistent
574 with previous findings (53,54), and their level in the *sir2*Δ mutant was ~30-fold greater than
575 that in WT cells (Fig. 2B, 2C). The level of IGS1-R transcripts was greater in all *caf-1*Δ mutants
576 than in WT cells, but not as high as those in the *sir2*Δ mutant (Fig. 2C). IGS1-F transcripts of
577 the size ranging from ~800 to ~1,200 nt were detected in the *sir2*Δ mutant at a level >10-fold
578 higher than that in WT cells (Fig. 2D, 2E), consistent with previous findings (53,54). Compared
579 to WT, the level of IGS1-F transcripts in *caf-1* mutants was higher, but the increase was less
580 pronounced than that in the *sir2*Δ mutant (Fig. 2D, 2E). For both the IGS1-R and IGS1-F
581 transcripts, *cac1*Δ and *cac2*Δ mutants showed stronger phenotypes than did the *cac3*Δ mutant
582 (Fig. 2B–2E). These results indicate that CAF-1 functions to repress transcription from E-pro,
583 but its contribution is smaller than that of Sir2.
584 To test the causal relationship between transcription from E-pro and rDNA instability
585 in the *caf-1* mutant, we used the strain that was engineered to have a galactose-inducible, bi-
586 directional *GAL1/10* promoter in place of E-pro in all the rDNA copies, which is hereafter
587 referred to as the Gal-pro strain (Fig. 2F) (24). In Gal-pro WT, *cac1*Δ, and *sir2*Δ strains,
588 transcription from the *GAL1/10* promoter was maintained at an extremely low level when cells
589 were grown in the presence of raffinose but was induced when galactose was added to the media
590 (Fig. 2G, 2H). ERC production was strongly suppressed in both the WT and *sir2*Δ mutant
591 strains in the Gal-pro background when grown in the presence of raffinose (Fig. 2I, 2J). In

592 contrast, in the Gal-pro *cac1*Δ mutant, the level of ERCs was ~4-fold higher than that in the
593 Gal-pro WT strain in the presence of raffinose, where IGS1-R transcripts were not detected
594 (Fig. 2G–2J, Gal-pro *cac1*Δ in raffinose vs. Gal-pro WT in raffinose). Thus, defects that were
595 independent of enhanced transcription near the RFB contributes to ERC production in the
596 *cac1*Δ mutant.

597 The addition of galactose to the media induced ERC production by 8- and 12-fold in
598 the Gal-pro WT and *sir2*Δ mutant strains, respectively, compared to the same strains when
599 grown in the presence of raffinose (Fig. 2I, 2J). This indicates that ERC production in WT and
600 *sir2*Δ mutant predominantly depends on the transcriptional activity near the RFB, consistent
601 with previous findings (24,55). In the Gal-pro *cac1*Δ mutant, the addition of galactose to the
602 media induced ERC production by ~3-fold, compared to that when grown in the raffinose-
603 containing media, but the degree of its induction was lower than that in the Gal-pro WT and
604 *sir2*Δ cells (Fig. 2I, 2J). Taken together, these findings suggest that CAF-1 stabilizes the rDNA
605 in a manner that is both dependent and independent through its function to repress transcription
606 at the E-pro locus.

607

608 **CAF-1 suppresses end resection of replication-coupled DSBs in the rDNA.**

609 To test whether enhanced E-pro activity resulted in cohesin dissociation from the CAR, we
610 conducted chromatin immunoprecipitation and quantitative PCR in WT, *cac1*Δ and *sir2*Δ
611 strains expressing the cohesin subunit Mcd1 tagged with a Flag epitope tag (Fig. 3A). Cohesin
612 was associated with the positive control region near a centromere on chr VI (Fig. 3B) (56), but
613 not with the negative control region near *YEL008W* on chr V (Fig. 3C), where cohesin
614 association was not observed in a previous chromatin immunoprecipitation sequencing study
615 (57). In the rDNA region, cohesin was most enriched in the CAR in exponentially growing WT
616 cells, and cohesin association was decreased in the *sir2*Δ mutant (Fig. 3A, ii), consistent with
617 previous findings (10). Although the *cac1*Δ mutant showed enhanced transcription from E-pro,
618 compared to that in WT cells (Fig. 2B–2E), it did not result in the inhibition of cohesin
619 association with the CAR (Fig. 3A).

620 We next examined whether CAF-1 impacts DSB formation and its repair by conducting
621 time course experiments during synchronous S phase progression in cells expressing the *FOB1*
622 gene under the control of the *GAL1* promoter (Fig. S2A). We prepared genomic DNA, digested
623 it with Bgl II (Fig. 3D), and separated it by conventional agarose gel electrophoresis, followed
624 by detection of arrested forks, DSBs, and resected DSBs by Southern blotting (Fig. 3E). The
625 DSB frequency was estimated by normalizing the maximum level of DSBs relative to that of
626 arrested forks in each time course. CAF-1 deficiency did not significantly impact DSB levels
627 (Fig. 3F).
628 The frequency of DSB end resection was determined by normalizing the maximum
629 level of resected DSB signal to that of DSBs in each time course. Consistent with our previous
630 finding (23), the absence of Sir2 led to a ~7-fold increase in the frequency of DSB end resection
631 (Fig. 3G). Cells lacking any subunits of CAF-1 showed ~2–3-fold increase in the frequency of
632 DSB end resection, compared to that in WT cells, but this increase was not as extensive as that
633 seen in cells lacking Sir2 (Fig. 3G). Because *GAL-FOB1* WT and *caf-1* mutants showed
634 comparable synchrony and timing in their progression through S phase (Supplementary Fig.
635 S2B), enhanced DSB end resection in *GAL-FOB1 caf-1* mutants was unlikely caused by
636 differences in the efficiency of release from G1 arrest by alpha factor. Taken together, these
637 findings suggest that CAF-1 suppresses end resection of DSBs formed at the RFB.
638
639 **The MRX complex is important for DSB repair and ERC production in the *caf-1* mutant.**
640 The MRX complex, along with its cofactor Sae2, initiates short-range end resection of double-
641 ended DSBs introduced by endonucleases, and Exo and Sgs1-Dna2 carry out long-range
642 resection (15,58,59). When *MRE11* or *SAE2* was deleted from *GAL-FOB1 cac1*Δ cells, resected
643 DSBs were barely detectable at the RFB (Fig. 4A and 4D, Supplementary Fig. S3A and S3D).
644 Therefore, the MRX complex and Sae2 are responsible for initiating end resection of
645 replication-coupled DSBs at the RFB in the *cac1*Δ mutant.
646 In *GAL-FOB1* WT cells, DSB signal appeared and disappeared at the timing similar to
647 that of arrested fork signal (Fig. 3E, 3H). *GAL-FOB1 cac1*Δ cells also showed efficient DSB

648 repair, as the timing of disappearance of DSB signal was similar to that of arrested fork signal
649 (Fig. 3I). On the contrary, in *GAL-FOB1* cells lacking Mre11, DSBs accumulated at the end of
650 time courses when most cells had completed bulk DNA synthesis and arrested forks had almost
651 disappeared (Fig. 4A, 4B and Supplementary Fig. S3A, S3B), consistent with a previous finding
652 (17,23). *GAL-FOB1 cac1*Δ *mre11*Δ cells also showed accumulation of DSBs at the end of time
653 courses (Fig. 4A, 4C and Supplementary Fig. S3A, S3C). When *SAE2* was deleted from *GAL-*
654 *FOB1* WT and *cac1*Δ cells, there was a slight delay in the disappearance of DSB signals,
655 compared to that of arrested fork signals, but DSB signals gradually decreased by the end of
656 time course, unlike DSBs that remained accumulated in cells lacking Mre11 (Fig. 4A–4F and
657 Supplementary Fig. S3). These findings demonstrate that the MRX complex is essential for
658 DSB repair but its function to carry out DSB end resection may be less important for DSB
659 repair.

660 Enhanced ERC production in the *cac2*Δ mutant was suppressed by deletion of *MRE11*
661 to the level seen in the *mre11*Δ single mutant, which was comparable to or slightly lower than
662 that in WT (Fig. 4G, 4H). Exo1 and Sgs1-Dna2 function redundantly to carry out long-range
663 DSB end resection (15,60). ERC levels in the *cac2*Δ mutant appeared slightly lowered by
664 deletion of *SGS1* and *EXO1*, but this difference was not statistically significant (Fig. 4I, 4J).
665 Taken together, these findings suggest that the MRX complex is essential for DSB repair and
666 prevention of rDNA instability by limiting ERC production.

667

668 **The interaction of CAF-1 with PCNA is critical for rDNA stabilization.**

669 CAF-1 is known to be recruited through its interaction with PCNA and deposit histones onto
670 the newly synthesized DNA (31-33). To test whether this recruitment is important for CAF-1's
671 function in rDNA, we examined the effect of mutations that compromise the interaction
672 between CAF-1 and PCNA. We introduced an empty plasmid or plasmids carrying the *CAC1*
673 or *cac1-20* allele that had a mutation in the PCNA-binding motif of the Cac1 protein (61) and
674 analyzed rDNA stability by PFGE and ERC analyses.

675 The *cac1*Δ mutant transformed with an empty vector showed smeared chr XII bands,
676 while the *cac1*Δ mutant complemented with a plasmid carrying *CAC1* showed sharp bands (Fig.
677 5A). Expression of *cac1-20* in the *cac1*Δ mutant resulted in chr XII bands that appeared less
678 smeared than those in the *cac1*Δ mutant with an empty vector, although the bands were still
679 broader than those in the *cac1*Δ mutant expressing *CAC1* (Fig. 5A). Expression of *CAC1* led to
680 lowering the level of ERCs in the *cac1*Δ mutant carrying an empty plasmid. However,
681 expression of *cac1-20* in the *cac1*Δ mutant did not cause a reduction in the ERC level, compared
682 to that in the *cac1*Δ mutant expressing *CAC1* (Fig. 5B, 5C). Therefore, the *cac1-20* mutant
683 defective in its binding to PCNA displayed rDNA instability. As the level of Cac1-20 was
684 comparable to that of Cac1 (Fig. 5D, 5E), enhanced rDNA instability in the *cac1-20* mutants
685 was unlikely caused by reduced expression due to its mutation.

686 We also analyzed the effects of three mutations in *POL30*, which encodes PCNA:
687 *pol30-6*, *pol30-8*, and *pol30-79*, all of which results in a substantial loss of the ability of PCNA
688 to bind to Cac1p (33). Because the *POL30* gene is essential, we constructed a diploid strain
689 heterozygous for *pol30*Δ, transformed it with plasmids carrying wild-type *POL30* or mutant
690 alleles, and isolated haploid *pol30*Δ mutants inheriting plasmids by tetrad dissection. In PFGE,
691 the *pol30*Δ mutant complemented with *POL30* showed sharp chr XII bands, but the *pol30*Δ
692 mutants expressing *pol30-6*, *pol30-8* or *pol30-79* showed smeared chr XII bands (Fig. 5F).
693 Moreover, compared with the *pol30*Δ mutant complemented with *POL30*, the *pol30*Δ mutants
694 expressing mutant alleles showed ~2.5-fold or even higher level of ERCs (Fig. 5G, 5H). rDNA
695 instability seen in these mutants was unlikely caused by reduced expression of these mutant
696 proteins, because the previous study demonstrated that the level of Pol30-6, Pol30-8 and Pol30-
697 79 proteins bound to chromatin are comparable to that of Pol30 (33). Taken together, these
698 findings suggest that the interaction of CAF-1 with PCNA, which is necessary for the
699 deposition of histones onto newly synthesized DNA, is important for the maintenance of rDNA
700 stability.
701

702 **CAF-1-mediated chromatin assembly facilitates properly spaced lagging strand synthesis**
703 **in the rDNA.**
704 During DNA replication *in vivo*, Okazaki fragment synthesis is interlinked with chromatin
705 assembly (39). Thus, analysis of Okazaki fragments allows us to assess nucleosome assembly
706 *in vivo*. To evaluate Okazaki fragment synthesis in the rDNA region, we used the strains
707 carrying a doxycycline-repressible allele of *CDC9* that encodes a DNA ligase joining Okazaki
708 fragments, isolated genomic DNA from cultures where *CDC9* was either shut off or kept
709 expressed, and separated equal amounts of genomic DNA by agarose gel electrophoresis under
710 denaturing conditions, followed by Southern blotting with an rDNA probe.
711 Upon *CDC9* inhibition, WT cells showed a ladder of bands that appeared to be sized
712 according to the nucleosomal repeat (165 bp) (Fig. 6A and Supplementary Fig. S4), consistent
713 with a previous finding that analyzed Okazaki fragments generated during bulk DNA synthesis
714 (39). When CAF-1 subunits were absent, overall lane signals were reduced, compared to those
715 seen in WT, even though equal amounts of DNA were loaded (Fig. 6A and Supplementary Fig.
716 S4). Previous studies analyzing bulk DNA demonstrated that the absence of CAF-1 subunits
717 completely abolishes the nucleosome-sized periodicity of Okazaki fragments and increases the
718 average length of Okazaki fragments (39-41). However, in our analysis that analyzed the
719 rDNA-specific effect, we still observed periodic signal peaks in *caf-1* mutants at the reduced
720 intensity, compared to those in WT (Fig. 6A and Supplementary Fig. S4). Furthermore, we did
721 not observe clear evidence of lengthening of Okazaki fragments. Nonetheless, these results
722 indicate that the *caf-1* mutants exhibited partial defects in nucleosome assembly in the rDNA.
723
724 **DISCUSSIONS**
725 Eukaryotic organisms have evolved mechanisms that faithfully maintain genetic and epigenetic
726 information. CAF-1 is one of the factors involved in these processes and ensures the
727 coordination of DNA replication with chromatin assembly (62). In this study, we demonstrated
728 that the absence of CAF-1 caused frequent expansion and contraction of the chromosomal
729 rDNA array as well as enhanced ERC production (Fig. 1). CAF-1 is important for the rDNA

730 stability in *A. thaliana*, but *A. thaliana* lacking CAF-1 leads only to loss of rDNA copies and
731 does not produce ERCs (42-44). The reasons behind these differences remain unclear. rDNA
732 instability in budding yeast *caf-1* mutants depends on Rad52 (Fig. 1F–1H), extending insights
733 from previous studies in *A. thaliana* (43). rDNA instability in budding yeast also depends on
734 Fob1 that is responsible for replication fork arrest at the RFB and subsequent DSB formation
735 (Fig. 1F–1H). Our findings suggest that CAF-1 suppresses HR-mediated chromosomal and
736 extrachromosomal rDNA instability during the repair of DSBs formed in the context of arrested
737 replication forks at the RFB.

738 CAF-1 is involved in silencing noncoding RNA transcription from the endogenous E-
739 pro (Fig. 2B–2E). Using Gal-pro *caf-1* mutants, we showed that the activation of transcription
740 at the E-pro locus induces ERC production, but these mutants produce ERCs even when this
741 transcription was kept low. Therefore, CAF-1 stabilizes the rDNA in a manner dependent and
742 independent through its function to repress transcription from E-pro (Fig. 2F–2J).

743 Previous studies demonstrate that the activation of transcription at the E-pro locus
744 prevents cohesin binding to the rDNA (10,23,24). Because a temperature-sensitive mutant of
745 *smc1*, which encodes one of the cohesin subunits, shows frequent loss of a marker gene from
746 the rDNA cluster, a previous model proposes that cohesins bound to the CAR and RFB
747 contribute to restricting the interaction of the DSB end with the misaligned rDNA copy during
748 DSB repair (10). Unexpectedly, the *cac1*Δ mutant, which showed a ~4-fold increase in the
749 transcription level at the E-pro locus (Fig. 2B–2E), did not show reduced cohesin binding but
750 rather showed a slight increase in cohesin binding to the rDNA (Fig. 3A), indicating that this
751 enhanced transcription is unlikely to affect rDNA instability through regulation of cohesion
752 associations. However, it is known that Eco1-dependent acetylation of a cohesin-subunit Smc3,
753 which is essential for cohesion establishment, is reduced in the *caf-1* mutant (63). Therefore,
754 we cannot exclude the possibility that CAF-1 is involved in the conversion of cohesin bound to
755 the rDNA locus into its establishment mode to stabilize the rDNA.

756 CAF-1 deficiency led to increased DSB end resection (Fig. 3E, 3G). We previously
757 demonstrated by analyzing the *sir2*Δ mutant that transcription activation at the E-pro locus

758 induces the collision of transcription machineries to the arrested replication forks at the RFB,
759 which recruits Mre11 and induces DSB end resection (23). Therefore, derepression of
760 transcription from E-pro in the *cac1*Δ mutant most likely contribute to enhanced DSB end
761 resection (Fig. 2B–2E, 3F). Alternatively, it is possible that chromatin assembled by CAF-1 at
762 the DSB may prevent DSB end resection by restricting the access by DSB end resection
763 enzymes. The MRX complex was required for DSB end resection, DSB repair, and ERC
764 production in the *caf-1* mutant, but ERC production in the *caf-1* mutant was not affected or
765 only slightly reduced, if any at all, by absence of both Exo1 and Sgs1 (Fig. 4). Thus, long-range
766 resection was not the absolute requirement for ERC production.

767 CAF-1 prevents Rad52-mediated rDNA instability during repair of replication-coupled
768 DSB repair at the RFB (Fig. 1F–1H). Knockdown of CAF-1 and another histone chaperone
769 ASF1 in human U-2 OS cells leads to reduced HR in response to replication-independent DSBs
770 introduced by an endonuclease I-SceI as well as reduced foci of Rad51 and its loader MMS22L-
771 TONSL upon treatment with DNA damaging agent bleomycin, leading to the model that CAF-
772 1 promotes proper chromatin assembly onto resected DSB ends to promote HR by facilitating
773 Rad51 loading onto resected DSBs (37). The function of CAF-1 in rDNA appears to contrast
774 to that of human CAF-1 in response to replication-independent DSBs, because CAF-1 prevents
775 rDNA recombination (Fig. 1F–1H). Knockdown of ASF1 in human cells additionally shows
776 increased levels of resected DSBs upon bleomycin treatment (37). Thus, human ASF1 is
777 involved in preventing DSB end resection, but it remains to be tested whether CAF-1 also elicit
778 similar function. A recent study in budding yeast has developed a system to introduce
779 replication-coupled DSBs using a Cas9 nickase (21). Absence of Asf1 causes severe growth
780 defects, when replication-dependent DSBs are introduced in the non-rDNA region by Cas9
781 nickase and guide RNA. CAF-1 deficiency reduces cellular growth but only when combined
782 with another histone chaperone Rtt106 (21). Thus, budding yeast CAF-1 plays a minor role in
783 response to replication-coupled DSBs caused by nicks on the template DNA. These findings
784 raise the possibility that CAF-1 elicits distinct functions in DSB repair, depending on the
785 sources of DSBs.

786 How does CAF-1 promote rDNA stability independently through its regulation of
787 transcription from E-pro? We analyzed Okazaki fragments during rDNA replication to assess
788 chromatin assembly around the RFB and found that abundance of nucleosome-sized Okazaki
789 fragments decreased in the *cac1*Δ mutant (Fig. 6A and Supplementary Fig. S4), indicating that
790 the nucleosome occupancy behind arrested forks and thus around DSBs at the RFB decreases
791 when CAF-1 is absent (Fig. 6B). CAF-1-mediated assembly of nucleosomes on newly
792 replicated DNA may be important for restricting DSB end resection and preventing the repair
793 of DSBs with the misaligned copy, which needs to be examined in future studies.
794 CAF-1 loads newly synthesized histones H3-H4, where histone H3K56 is acetylated
795 by the histone chaperone Rtt109 (28-30). Defective acetylation of histone H3K56 renders cells
796 sensitive to DNA damaging agents, suggesting that chromatin with histone H3K56 acetylation
797 facilitates DNA repair (29). We previously demonstrated that the absence of Rtt109, which is
798 responsible for the acetylation of histone H3K56, induces rDNA instability (35). We speculate
799 that during DSB repair, Rad52 preferentially uses a homologous rDNA copy that contains
800 chromatin with acetylated histone H3K56 (Fig. 6B). Deficiency of CAF-1 results in defects in
801 the deposition of nucleosomes with acetylated histone H3K56 on replicating DNA (Fig. 6B,
802 right). Defective nucleosome assembly may derepress transcription from E-pro, which
803 contributes to enhanced DNA end resection and Rad52-mediated repair. The likelihood of
804 having acetylated histone H3K56 is low behind the arrested forks at the RFB. Thus, in cells
805 lacking CAF-1, Rad52 is unlikely to use the rDNA copy at an aligned position for DSB repair
806 due to the absence of H3K56 acetylation but instead preferentially uses a copy that is distant
807 from the DSB site, leading to chromosomal rDNA copy number changes and ERC production
808 (Fig. 6B). Defects in proper assembly of chromatin with H3K56 acetylation may promote
809 frequent usage of the misaligned copy during DSB repair, independently of the transcription
810 status at the E-pro.
811

Data availability

All data are available upon request.

Acknowledgements

We are grateful to Peter Burgers for the plasmids pBL230-0, 6, 8 and 79 and Iestyn Whitehouse for the yIW310 strain. We thank Etsuko Imatani and Akemi Mizuguchi for technical assistances and members of the Kobayashi and Sasaki laboratories for discussions.

Author contributions: T.K. and M.S. conceived the research. H.F., M.S. and T.K. designed the experiments and analyzed the data. H.F., T.Y., Y.K., N.A., and M.S. performed the experiments. M.S. wrote the manuscript with input from T.K.

Funding

Japan Society for the Promotion of Science [20H05382 and 24K09417 to M.S. and 17H01443 and 21H04761 to T.K.]; Japan Science and Technology Agency Fusion Oriented REsearch for disruptive Science and Technology, FOREST [JPMJFR214P to M.S.]; Naito Foundation (to M.S.); Japan Agency for Medical Research and Development [JP21gm1110010 to T.K.]; Core Research for Evolutional Science and Technology [JPMJCR19S3 to T.K.], Strategic Research Projects grant from Research Organization of Information and Systems.

Conflict of interest statement

None declared.

834 **Figure Legends**

835 **Figure 1. CAF-1 suppresses HR-mediated rDNA instability in response to Fob1-**
836 **dependent replication fork arrest.**

837 **(A)** Replication fork arrest, DSB formation, and rDNA copy number changes in the budding
838 yeast rDNA region. Chr XII carries the rDNA cluster, as indicated by the green bar, where
839 approximately 150 rDNA copies are tandemly arrayed. Each copy contains 35S rRNA (35S),
840 5S rRNA (5S), an origin of DNA replication (Ori), a cohesin-associated region (CAR), a
841 bidirectional promoter for noncoding RNA, called E-pro, and a replication fork barrier (RFB).
842 The black bar indicates the position of probe 1 used for ERC detection.

843 **(B, F)** PFGE analysis of chr XII size heterogeneity. DNA from three independent clones (B)
844 and four independent clones (F) of the indicated strains was separated by PFGE and stained
845 with ethidium bromide (EtBr). M indicates *Hansenula wingei* chromosomal DNA markers.

846 **(C, G)** ERC detection. DNA was isolated from two independent clones (C) and four
847 independent clones (G) of the indicated strains and separated by agarose gel electrophoresis,
848 followed by Southern blotting with the probe 1, as shown in (A). In (G), DNA from the first
849 WT clone (WT-1) run on the left gel was also loaded on the right gel. Chromosomal rDNA and
850 different ERC forms are indicated. rl and sc indicate relaxed and supercoiled forms of ERCs,
851 respectively. Supercoiled monomers ran off from the gel in the electrophoresis condition used
852 in this experiment. M indicates lambda Hind III DNA markers. The top panel shows short
853 exposure of genomic rDNA signals.

854 **(D, H)** Quantitation of ERCs. ERCs from (C) and Supplementary Figure 1A were quantified in
855 (D). ERCs from (G) were quantified in (H). ERC levels were compared between WT and
856 mutants by one-way ANOVA, followed by Tukey's multiple comparisons test. Bars show the
857 mean ± s.e.m. Asterisks indicate statistically significant differences between WT and mutant
858 strains ($p < 0.05$).

859 **(E)** Proportion of different ERC forms. In each sample, monomeric, dimeric and multimeric
860 ERCs were quantified and the proportion of each form in total was expressed as proportion of
861 total ERCs.

862

863 **Figure 2. CAF-1 stabilizes the rDNA through both E-pro transcription-dependent and -**
864 **independent mechanisms.**

865 **(A, F)** Positions of probes 2 and 3 used for the detection of noncoding RNA by Northern
866 blotting in strains carrying the native E-pro (A) or Gal-pro (F).

867 **(B, D, G)** Northern blot analysis of noncoding RNAs transcribed from the intergenic regions in
868 the rDNA. Total RNA was isolated from three independent clones of strains carrying E-pro (B,
869 D) and two independent clones of Gal-pro strains grown in the presence of either raffinose or
870 galactose in the media (G). RNA was separated by size on formaldehyde-agarose gels, followed
871 by Northern blotting. In (B) and (G), IGS1-R transcripts were detected with probe 2. In (D),
872 IGS1-F transcripts were detected with probe 3. The membranes were reprobed for *TSA1*
873 transcripts as a control for loading.

874 **(C, E, H)** Quantitation of noncoding RNA. In (C) and (E), signals corresponding to IGS1-R
875 transcripts in (B) and IGS1-F transcripts in (D) were quantified relative to *TSA1*, respectively,
876 which were normalized to the average of WT clones. In (H), IGS1-F transcripts were
877 normalized to *TSA1* and expressed relative to the average of Gal-pro WT clones grown in the
878 presence of galactose. Bars show the mean ± s.e.m. (C, E) and the mean and the range from
879 two independent experiments (H). Transcript levels were compared by one-way ANOVA,
880 followed by Tukey's multiple comparisons test (C, E); *, statistically significant difference
881 between WT and mutants ($p < 0.05$); ns, no significant difference ($p > 0.05$).

882 **(I)** ERC detection. DNA was isolated from independent clones of the indicated strains in the
883 Gal-pro background and separated by agarose gel electrophoresis, followed by Southern
884 blotting with the probe 1, as shown in Fig. 1A. Chromosomal rDNA and different forms of
885 ERCs are indicated. rl and sc indicate relaxed and supercoiled ERCs, respectively. Supercoiled
886 monomers ran off from the gel in the electrophoresis condition under these conditions. The
887 sizes of lambda Hind III DNA markers are indicated. The top panel shows a short exposure of
888 chromosomal rDNA signals.

889 **(J)** Quantitation of ERCs. ERCs were quantified from three independent clones of the indicated
890 strains, including two clones in (H) and a third clone analyzed on a separate gel. ERC levels
891 were compared by the two-sided Student's t-tests. Bars show the mean ± s.e.m. Asterisks above
892 brackets indicate statistically significant differences between strains that were grown in the
893 indicated growth conditions ($p < 0.05$).
894
895 **Figure 3. CAF-1 suppresses DSB end resection.**
896 **(A, B, C)** ChIP–qPCR analyses of Mcd1-Flag in the indicated strains. The regions where
897 cohesin enrichments were examined are indicated as black bars. Four different regions in the
898 rDNA region (i)–(iv) in (A), the positive control region near *CEN6* in (B) and the negative
899 control region near *YEL088W* on chr V (C) were examined. Untagged strains were used as
900 controls. ChIP was performed using an antibody against a Flag epitope tag. The enrichment of
901 chromatin in the indicated regions is expressed as the % input (IP/whole-cell extract). The bars
902 show the mean ± s.e.m. from three independent cultures of each strain.
903 **(D)** Restriction map and the positions of the probe 4 used for DSB analyses. The restriction
904 sites for Bgl II (Bg) are indicated.
905 **(E)** DSB assay. Time-course experiments were conducted by arresting the indicated strains in
906 the *GAL-FOB1* background in G1 with alpha factor, releasing cells into fresh media and
907 collecting cells at different time points, as described in Supplementary Fig. S2A. Genomic DNA
908 was isolated, digested with Bgl II, separated by size, and analyzed by Southern blotting with
909 probe 4, as shown in (D). Arrested forks, linear fragments, DSBs and resected DSBs are
910 indicated. Terminal fragments indicate the telomere-proximal rDNA repeat. Long exposure
911 panels around DSBs and resected DSBs are shown below.
912 **(F)** Quantitation of DSBs. The frequency of DSBs was determined by quantifying the
913 maximum signal of DSBs relative to the maximum signal of arrested forks in each time course.
914 The average DSB frequency from three independent time course experiments was determined
915 and normalized to the average of WT clones (bars show the mean ± s.e.m.). Multiple
916 comparisons were performed by one-way ANOVA, followed by Tukey's multiple comparisons

917 test. The difference in DSB frequencies between WT and all other mutants was not statistically
918 significant.
919 **(G)** Quantitation of resected DSBs. The frequency of resected DSB was determined by
920 quantifying the maximum signal of resected DSBs relative to the maximum signal of DSBs in
921 each time course. The average frequency of resected DSBs from three independent time course
922 experiments was determined and normalized to the average of WT clones (bars show the mean
923 ± s.e.m.). Multiple comparisons were performed by one-way ANOVA, followed by Tukey's
924 multiple comparisons test; *, statistically significant difference ($p < 0.05$).
925 **(H, I)** Timing of appearance and disappearance of arrested forks and DSBs. Arrested forks and
926 DSBs are expressed as percent of maximum values in one of the three independent time course
927 experiments of *GAL-FOB1* WT (H) and *cac1*Δ strains (I).
928
929 **Figure 4. The MRX complex is required for DSB repair and ERC production in the *caf-1***
930 **mutant.**
931 **(A, D)** DSB assay. Time-course experiments were conducted by arresting the indicated strains
932 in the *GAL-FOB1* background in G1 with alpha factor, releasing cells into fresh media and
933 collecting cells at different time points, as described in Supplementary Fig. S2A. Genomic DNA
934 was isolated, digested with Bgl II, separated by size, and analyzed by Southern blotting with
935 probe 4, as shown in Fig. 3D. Arrested forks, linear fragments, DSBs, and resected DSBs are
936 indicated. Terminal fragments indicate the telomere-proximal rDNA repeat. Long exposure
937 panels around DSBs and resected DSBs are shown below.
938 **(B, C, E, F)** Timing of appearance and disappearance of arrested forks and DSBs. Arrested
939 forks and DSBs are expressed as percent of maximum values in one of the two independent
940 time course experiments of the indicated strains.
941 **(G, I)** ERC detection. DNA was isolated from four independent clones (G) and three
942 independent clones (J) of the indicated strains and separated by agarose gel electrophoresis,
943 followed by Southern blotting with the probe 1, as shown in Fig. 1A. Chromosomal rDNA and
944 different forms of ERCs are indicated. rl and sc indicate relaxed and supercoiled ERCs,

945 respectively. The sizes of lambda Hind III DNA markers are indicated. The top panel shows a
946 short exposure of chromosomal rDNA signals.
947 **(H, J)** Quantitation of ERCs. In (H) and (J), ERCs were quantified from (G) and (I), respectively.
948 ERC levels were compared between WT and mutants by one-way ANOVA, followed by
949 Tukey's multiple comparisons test. Bars show the mean ± s.e.m. Asterisks indicate statistically
950 significant differences between WT and mutant strains ($p < 0.05$). ns indicates no significant
951 difference ($p > 0.05$).
952
953 **Figure 5. Interaction with PCNA is important for CAF-1 to stabilize the rDNA.**
954 **(A, F)** PFGE analysis to examine the size heterogeneity of chr XII. DNA from independent
955 clones of the indicated strains was separated by PFGE and stained with EtBr. M indicates *H.*
956 *wingei* chromosomal DNA markers.
957 **(B, G)** ERC detection. DNA was isolated from 6 independent clones (B) and four independent
958 clones (G) of the indicated strains and separated by agarose gel electrophoresis, followed by
959 Southern blotting with the probe 1, as shown in Fig. 1A. Genomic rDNA and different forms
960 of ERCs are indicated. M indicates lambda Hind III DNA markers. The top panel shows a short
961 exposure of genomic rDNA signals.
962 **(C, H)** Quantitation of ERC levels. ERCs in (B, G) were quantified and their levels were
963 normalized to those of the *cac1*Δ strain complemented with a plasmid carrying *CAC1* in (C)
964 and the *pol30*Δ strain complemented with a plasmid carrying *POL30* in (H). ERC levels among
965 different strains were compared by one-way ANOVA, followed by Tukey's multiple
966 comparisons test. Bars show the mean ± s.e.m. Asterisks above bars and above brackets indicate
967 statistically significant differences between WT and mutant strains and between mutant strains,
968 respectively ($p < 0.05$). ns indicates no significant difference ($p > 0.05$).
969 **(D)** Western blot of Cac1 that is C-terminally tagged with a nine Myc epitope and tubulin from
970 four independent clones of the *cac1*Δ strains that were transformed with a YCp22 vector or the
971 vectors expressing either Cac1-9myc or Cac1-20-9myc.

972 **(E)** Quantitation of Cac1-myc protein levels. The levels of Cac1-9myc and Cac1-20-9myc were
973 quantified in the indicated strains relative to tubulin, which was normalized to the average of
974 the *cac1*Δ clones expressing Cac1-9myc. Bars show the mean ± s.e.m. Multiple comparisons
975 were performed by one-way ANOVA, followed by Tukey's multiple comparisons test; *,
976 statistically significant difference ($p < 0.05$); ns, no significant difference ($p > 0.05$).
977
978 **Figure 6. A model for CAF-1-mediated rDNA stabilization.**
979 **(A)** The size of Okazaki fragments generated during rDNA replication. WT, *cac1*Δ, *cac2*Δ,and
980 *cac3*Δ cells carrying a doxycycline-repressible allele of *CDC9* were treated or not treated with
981 doxycycline (Dox). Genomic DNA was isolated and separated on a denaturing agarose gel,
982 followed by Southern blotting with a rDNA probe 1, as indicated in Fig. 1A. Lane profiles of
983 the indicated strains, in which *CDC9* was shut off, were included. The positions of the bands
984 of Okazaki fragments are indicated by arrowheads.
985 **(B)** A model for CAF-1-mediated rDNA stabilization. Left: CAF-1 facilitates nucleosome
986 assembly onto replicating DNA by depositing a newly synthesized $(H3\text{-}H4)_2$ tetramer where
987 H3K56 is acetylated (Ac). The assembly of the properly spaced nucleosome leads to the
988 repression of transcription from E-pro. DSBs formed in this chromatin environment are
989 repaired in a manner that does not involve rDNA copy number changes. Right: The absence of
990 CAF-1 leads to defects in depositing newly synthesized histones. This environment results in
991 the activation of transcription from E-pro, leading to the induction of DSB end resection and
992 HR-mediated DSB repair. The HR protein Rad52 bound to resected DSBs preferentially uses
993 the rDNA copy in a chromatin environment with histone H3K56Ac. Because the density of
994 histone H3 acetylated at K56 is low in the CAF-1-defective strain, Rad52 assembled on the
995 replicated DNA preferentially uses the distant rDNA copy, inducing rDNA instability. This
996 template choice error may not be affected by transcription at the E-pro.
997

998 **Supplementary Figure 1. ERC detection in the *caf-1* mutants.**

999 **(A, B, D)** ERC detection. DNA was isolated from the two independent clones (A) and four
1000 independent clones (B, D) of the indicated strains and separated by agarose gel electrophoresis,
1001 followed by Southern blotting with the probe 1, as shown in Fig. 1A. Chromosomal rDNA and
1002 different forms of ERCs are indicated. rl and sc indicate relaxed and supercoiled ERCs,
1003 respectively. Supercoiled monomers ran off from the gel in the electrophoresis condition under
1004 these conditions. The sizes of lambda Hind III DNA markers are indicated. The top panel shows
1005 a short exposure of chromosomal rDNA signals. The DNA sample that was indicated as WT-1
1006 was the same DNA sample isolated from the clone that was loaded a separate gel: WT-1 in (A)
1007 is the first WT clone in Fig. 1C; WT-1 in (B) is the first WT clone on the left gel; WT-1 in (D)
1008 is the first WT clone on the left gel. These DNA samples were used to normalize ERC levels in
1009 the mutants that were analyzed on separate gels.

1010 **(C, E)** Quantitation of ERCs. In (C) and (E), ERCs were quantified from (B) and (D),
1011 respectively. Multiple comparisons were performed by one-way ANOVA, followed by Tukey's
1012 multiple comparisons test; *, statistically significant difference ($p < 0.05$).

1013

1014 **Supplementary Fig. 2. Time course experiments to analyze formation and repair of DSBs.**

1015 **(A)** Outline of time course experiments.

1016 (B) Cell cycle analysis of two representative time course experiments using *GAL-FOB1* WT,
1017 *cac1*Δ, *cac2*Δ, *cac3*Δ, and *sir2*Δ strains by flow cytometry.

1018

1019 **Supplementary Figure 3. Time course experiments to analyze DSB repair in *cac1*Δ *mre11*Δ**
1020 **and *cac1*Δ *sae2*Δ.**

1021 **(A, D)** DSB assay. Time-course experiments were conducted, as described in Supplementary
1022 Fig. S2A. Genomic DNA was isolated, digested with Bgl II, separated by size, and analyzed by
1023 Southern blotting with probe 4, as shown in Fig. 3D. Arrested forks, linear fragments, DSBs
1024 and resected DSBs are indicated. Terminal fragments indicate the telomere-proximal rDNA
1025 repeat. Long exposure panels around DSBs and resected DSBs are shown below.

1026 **(B, C, E, F)** Arrested forks and DSBs are expressed as percent of maximum values in one of
1027 the two independent time course experiments of the indicated strains.
1028
1029 **Supplementary Figure 4. The size of Okazaki fragments in the *caf-1* mutants.**
1030 Okazaki fragments were analyzed in WT, *cac1*Δ, *cac2*Δ, and *cac3*Δ cells carrying a
1031 doxycycline-repressible allele of *CDC9* that were treated or not treated with doxycycline (Dox).
1032 Genomic DNA was isolated and separated on a denaturing agarose gel, followed by Southern
1033 blotting with probe 1, as indicated in Fig. 1A. Lane profiles of the indicated strains, in which
1034 *CDC9* was shut off, were included. The positions of the bands of Okazaki fragments are
1035 indicated by arrowheads.
1036

1037 **REFERENCES**

1038 1. Carvalho, C.M. and Lupski, J.R. (2016) Mechanisms underlying structural variant
1039 formation in genomic disorders. *Nat Rev Genet*, **17**, 224-238.

1040 2. Verhaak, R.G.W., Bafna, V. and Mischel, P.S. (2019) Extrachromosomal oncogene
1041 amplification in tumour pathogenesis and evolution. *Nat Rev Cancer*, **19**, 283-288.

1042 3. Yan, X., Mischel, P. and Chang, H. (2024) Extrachromosomal DNA in cancer. *Nature*
1043 *Reviews Cancer*.

1044 4. Sasaki, M., Lange, J. and Keeney, S. (2010) Genome destabilization by homologous
1045 recombination in the germ line. *Nat Rev Mol Cell Biol*, **11**, 182-195.

1046 5. Harel, T. and Lupski, J.R. (2018) Genomic disorders 20 years on-mechanisms for
1047 clinical manifestations. *Clin Genet*, **93**, 439-449.

1048 6. Brewer, B.J. and Fangman, W.L. (1988) A replication fork barrier at the 3' end of yeast
1049 ribosomal RNA genes. *Cell*, **55**, 637-643.

1050 7. Brewer, B.J., Lockshon, D. and Fangman, W.L. (1992) The arrest of replication forks
1051 in the rDNA of yeast occurs independently of transcription. *Cell*, **71**, 267-276.

1052 8. Kobayashi, T., Hidaka, M., Nishizawa, M. and Horiuchi, T. (1992) Identification of a
1053 site required for DNA replication fork blocking activity in the rRNA gene cluster in
1054 Saccharomyces cerevisiae. *Mol Gen Genet*, **233**, 355-362.

1055 9. Burkhalter, M.D. and Sogo, J.M. (2004) rDNA enhancer affects replication initiation
1056 and mitotic recombination: Fob1 mediates nucleolytic processing independently of
1057 replication. *Molecular cell*, **15**, 409-421.

1058 10. Kobayashi, T., Horiuchi, T., Tongaonkar, P., Vu, L. and Nomura, M. (2004) SIR2
1059 regulates recombination between different rDNA repeats, but not recombination within
1060 individual rRNA genes in yeast. *Cell*, **117**, 441-453.

1061 11. Weitao, T., Budd, M., Hoopes, L.L. and Campbell, J.L. (2003) Dna2 helicase/nuclease
1062 causes replicative fork stalling and double-strand breaks in the ribosomal DNA of
1063 Saccharomyces cerevisiae. *The Journal of biological chemistry*, **278**, 22513-22522.

1064 12. Sasaki, M. and Kobayashi, T. (2023) Regulatory processes that maintain or alter
1065 ribosomal DNA stability during the repair of programmed DNA double-strand breaks.
1066 *Genes Genet Syst*, **98**, 103-119.

1067 13. Paques, F. and Haber, J.E. (1999) Multiple pathways of recombination induced by
1068 double-strand breaks in Saccharomyces cerevisiae. *Microbiol Mol Biol Rev*, **63**, 349-
1069 404.

1070 14. Symington, L.S., Rothstein, R. and Lisby, M. (2014) Mechanisms and regulation of
1071 mitotic recombination in Saccharomyces cerevisiae. *Genetics*, **198**, 795-835.

1072 15. Cejka, P. and Symington, L.S. (2021) DNA End Resection: Mechanism and Control.
1073 *Annu Rev Genet*, **55**, 285-307.

1074 16. Pavani, R., Tripathi, V., Vrtis, K.B., Zong, D., Chari, R., Callen, E., Pankajam, A.V.,
1075 Zhen, G., Matos-Rodrigues, G., Yang, J. *et al.* (2024) Structure and repair of
1076 replication-coupled DNA breaks. *Science*, **385**, eado3867.

1077 17. Sasaki, M. and Kobayashi, T. (2017) Ctf4 Prevents Genome Rearrangements by
1078 Suppressing DNA Double-Strand Break Formation and Its End Resection at Arrested
1079 Replication Forks. *Molecular cell*, **66**, 533-545 e535.

1080 18. Cortes-Ledesma, F. and Aguilera, A. (2006) Double-strand breaks arising by replication
1081 through a nick are repaired by cohesin-dependent sister-chromatid exchange. *EMBO*
1082 *Rep*, **7**, 919-926.

1083 19. Gonzalez-Barrera, S., Cortes-Ledesma, F., Wellinger, R.E. and Aguilera, A. (2003)
1084 Equal sister chromatid exchange is a major mechanism of double-strand break repair
1085 in yeast. *Molecular cell*, **11**, 1661-1671.

1086 20. Jakobsen, K.P., Nielsen, K.O., Lovschal, K.V., Rodgaard, M., Andersen, A.H. and
1087 Bjergbaek, L. (2019) Minimal Resection Takes Place during Break-Induced
1088 Replication Repair of Collapsed Replication Forks and Is Controlled by Strand
1089 Invasion. *Cell Rep*, **26**, 836-844 e833.

1090 21. Kimble, M.T., Sane, A., Reid, R.J.D., Johnson, M.J., Rothstein, R. and Symington, L.S.
1091 (2024) Repair of replication-dependent double-strand breaks differs between the
1092 leading and lagging strands. *Molecular cell*.

1093 22. Mayle, R., Campbell, I.M., Beck, C.R., Yu, Y., Wilson, M., Shaw, C.A., Bjergbaek, L.,
1094 Lupski, J.R. and Ira, G. (2015) DNA REPAIR. Mus81 and converging forks limit the
1095 mutagenicity of replication fork breakage. *Science*, **349**, 742-747.

1096 23. Sasaki, M. and Kobayashi, T. (2025) Transcription near arrested DNA replication forks
1097 triggers ribosomal DNA copy number changes. *Nucleic Acids Res*, **53**.

1098 24. Kobayashi, T. and Ganley, A.R. (2005) Recombination regulation by transcription-
1099 induced cohesin dissociation in rDNA repeats. *Science*, **309**, 1581-1584.

1100 25. Laloraya, S., Guacci, V. and Koshland, D. (2000) Chromosomal addresses of the
1101 cohesin component Mcd1p. *J Cell Biol*, **151**, 1047-1056.

1102 26. Serra-Cardona, A. and Zhang, Z. (2018) Replication-Coupled Nucleosome Assembly
1103 in the Passage of Epigenetic Information and Cell Identity. *Trends Biochem Sci*, **43**,
1104 136-148.

1105 27. Stewart-Morgan, K.R., Petryk, N. and Groth, A. (2020) Chromatin replication and
1106 epigenetic cell memory. *Nat Cell Biol*, **22**, 361-371.

1107 28. Driscoll, R., Hudson, A. and Jackson, S.P. (2007) Yeast Rtt109 promotes genome
1108 stability by acetylating histone H3 on lysine 56. *Science*, **315**, 649-652.

1109 29. Masumoto, H., Hawke, D., Kobayashi, R. and Verreault, A. (2005) A role for cell-cycle-
1110 regulated histone H3 lysine 56 acetylation in the DNA damage response. *Nature*, **436**,
1111 294-298.

1112 30. Han, J., Zhou, H., Horazdovsky, B., Zhang, K., Xu, R.M. and Zhang, Z. (2007) Rtt109
1113 acetylates histone H3 lysine 56 and functions in DNA replication. *Science*, **315**, 653-
1114 655.

1115 31. Shibahara, K. and Stillman, B. (1999) Replication-dependent marking of DNA by
1116 PCNA facilitates CAF-1-coupled inheritance of chromatin. *Cell*, **96**, 575-585.

1117 32. Smith, S. and Stillman, B. (1989) Purification and characterization of CAF-I, a human
1118 cell factor required for chromatin assembly during DNA replication in vitro. *Cell*, **58**,
1119 15-25.

1120 33. Zhang, Z., Shibahara, K. and Stillman, B. (2000) PCNA connects DNA replication to
1121 epigenetic inheritance in yeast. *Nature*, **408**, 221-225.

1122 34. Duro, E., Vaisica, J.A., Brown, G.W. and Rouse, J. (2008) Budding yeast Mms22 and
1123 Mms1 regulate homologous recombination induced by replisome blockage. *DNA*
1124 *repair*, **7**, 811-818.

1125 35. Ide, S., Saka, K. and Kobayashi, T. (2013) Rtt109 prevents hyper-amplification of
1126 ribosomal RNA genes through histone modification in budding yeast. *PLoS Genet*, **9**,
1127 e1003410.

1128 36. Houseley, J. and Tollervey, D. (2011) Repeat expansion in the budding yeast ribosomal
1129 DNA can occur independently of the canonical homologous recombination machinery.
1130 *Nucleic Acids Res*, **39**, 8778-8791.

1131 37. Huang, T.H., Fowler, F., Chen, C.C., Shen, Z.J., Sleckman, B. and Tyler, J.K. (2018)
1132 The Histone Chaperones ASF1 and CAF-1 Promote MMS22L-TONSL-Mediated
1133 Rad51 Loading onto ssDNA during Homologous Recombination in Human Cells.
1134 *Molecular cell*, **69**, 879-892 e875.

1135 38. Li, Q., Zhou, H., Wurtele, H., Davies, B., Horazdovsky, B., Verreault, A. and Zhang, Z.
1136 (2008) Acetylation of histone H3 lysine 56 regulates replication-coupled nucleosome
1137 assembly. *Cell*, **134**, 244-255.

1138 39. Smith, D.J. and Whitehouse, I. (2012) Intrinsic coupling of lagging-strand synthesis to
1139 chromatin assembly. *Nature*, **483**, 434-438.

1140 40. Borges, V., Smith, D.J., Whitehouse, I. and Uhlmann, F. (2013) An Eco1-independent
1141 sister chromatid cohesion establishment pathway in S. cerevisiae. *Chromosoma*, **122**,
1142 121-134.

1143 41. Yadav, T. and Whitehouse, I. (2016) Replication-Coupled Nucleosome Assembly and
1144 Positioning by ATP-Dependent Chromatin-Remodeling Enzymes. *Cell Rep*, **15**, 715-
1145 723.

1146 42. Mozgova, I., Mokros, P. and Fajkus, J. (2010) Dysfunction of chromatin assembly
1147 factor 1 induces shortening of telomeres and loss of 45S rDNA in Arabidopsis thaliana.
1148 *Plant Cell*, **22**, 2768-2780.

1149 43. Muchova, V., Amiard, S., Mozgova, I., Dvorackova, M., Gallego, M.E., White, C. and
1150 Fajkus, J. (2015) Homology-dependent repair is involved in 45S rDNA loss in plant
1151 CAF-1 mutants. *Plant J*, **81**, 198-209.

1152 44. Pavlistova, V., Dvorackova, M., Jez, M., Mozgova, I., Mokros, P. and Fajkus, J. (2016)
1153 Phenotypic reversion in fas mutants of Arabidopsis thaliana by reintroduction of FAS
1154 genes: variable recovery of telomeres with major spatial rearrangements and
1155 transcriptional reprogramming of 45S rDNA genes. *Plant J*, **88**, 411-424.

1156 45. Sasaki, M. and Kobayashi, T. (2021) Gel Electrophoresis Analysis of rDNA Instability
1157 in Saccharomyces cerevisiae. *Methods Mol Biol*, **2153**, 403-425.

1158 46. Ayyagari, R., Impellizzeri, K.J., Yoder, B.L., Gary, S.L. and Burgers, P.M. (1995) A
1159 mutational analysis of the yeast proliferating cell nuclear antigen indicates distinct roles
1160 in DNA replication and DNA repair. *Molecular and cellular biology*, **15**, 4420-4429.

1161 47. Eissenberg, J.C., Ayyagari, R., Gomes, X.V. and Burgers, P.M. (1997) Mutations in
1162 yeast proliferating cell nuclear antigen define distinct sites for interaction with DNA
1163 polymerase delta and DNA polymerase epsilon. *Molecular and cellular biology*, **17**,
1164 6367-6378.

1165 48. Janke, C., Magiera, M.M., Rathfelder, N., Taxis, C., Reber, S., Maekawa, H., Moreno-
1166 Borchart, A., Doenges, G., Schwob, E., Schiebel, E. *et al.* (2004) A versatile toolbox
1167 for PCR-based tagging of yeast genes: new fluorescent proteins, more markers and
1168 promoter substitution cassettes. *Yeast*, **21**, 947-962.

1169 49. Iida, T. and Kobayashi, T. (2019) RNA Polymerase I Activators Count and Adjust
1170 Ribosomal RNA Gene Copy Number. *Molecular cell*, **73**, 645-654 e613.

1171 50. Saka, K., Takahashi, A., Sasaki, M. and Kobayashi, T. (2016) More than 10% of yeast
1172 genes are related to genome stability and influence cellular senescence via rDNA
1173 maintenance. *Nucleic Acids Res*.

1174 51. Sauty, S.M. and Yankulov, K. (2023) Analyses of POL30 (PCNA) reveal positional
1175 effects in transient repression or bi-modal active/silent state at the sub-telomeres of S.
1176 cerevisiae. *Epigenetics Chromatin*, **16**, 40.

1177 52. Smith, J.S., Caputo, E. and Boeke, J.D. (1999) A genetic screen for ribosomal DNA
1178 silencing defects identifies multiple DNA replication and chromatin-modulating
1179 factors. *Molecular and cellular biology*, **19**, 3184-3197.

1180 53. Hosoyamada, S., Sasaki, M. and Kobayashi, T. (2019) The CCR4-NOT Complex
1181 Maintains Stability and Transcription of rRNA Genes by Repressing Antisense
1182 Transcripts. *Molecular and cellular biology*, **40**.

1183 54. Houseley, J., Kotovic, K., El Hage, A. and Tollervey, D. (2007) Trf4 targets ncRNAs
1184 from telomeric and rDNA spacer regions and functions in rDNA copy number control.
1185 *EMBO J*, **26**, 4996-5006.

1186 55. Saka, K., Ide, S., Ganley, A.R. and Kobayashi, T. (2013) Cellular senescence in yeast
1187 is regulated by rDNA noncoding transcription. *Curr Biol*, **23**, 1794-1798.

1188 56. Gruber, S., Arumugam, P., Katou, Y., Kuglitsch, D., Helmhart, W., Shirahige, K. and
1189 Nasmyth, K. (2006) Evidence that loading of cohesin onto chromosomes involves
1190 opening of its SMC hinge. *Cell*, **127**, 523-537.

1191 57. Pakchuen, S., Ishibashi, M., Takakusagi, E., Shirahige, K. and Sutani, T. (2016)
1192 Physical Association of Saccharomyces cerevisiae Polo-like Kinase Cdc5 with
1193 Chromosomal Cohesin Facilitates DNA Damage Response. *The Journal of biological*
1194 *chemistry*, **291**, 17228-17246.

1195 58. Cannavo, E. and Cejka, P. (2014) Sae2 promotes dsDNA endonuclease activity within
1196 Mre11-Rad50-Xrs2 to resect DNA breaks. *Nature*, **514**, 122-125.

59. Cannavo, E., Reginato, G. and Cejka, P. (2019) Stepwise 5' DNA end-specific resection of DNA breaks by the Mre11-Rad50-Xrs2 and Sae2 nuclease ensemble. *Proceedings of the National Academy of Sciences of the United States of America*, **116**, 5505-5513.

60. Mimitou, E.P. and Symington, L.S. (2009) DNA end resection: many nucleases make light work. *DNA repair*, **8**, 983-995.

61. Krawitz, D.C., Kama, T. and Kaufman, P.D. (2002) Chromatin assembly factor I mutants defective for PCNA binding require Asf1/Hir proteins for silencing. *Molecular and cellular biology*, **22**, 614-625.

62. Sauer, P.V., Gu, Y., Liu, W.H., Mattiroli, F., Panne, D., Luger, K. and Churchill, M.E. (2018) Mechanistic insights into histone deposition and nucleosome assembly by the chromatin assembly factor-1. *Nucleic Acids Res*, **46**, 9907-9917.

63. Ghaddar, N., Luciano, P., Geli, V. and Corda, Y. (2023) Chromatin assembly factor-1 preserves genome stability in ctf4Delta cells by promoting sister chromatid cohesion. *Cell Stress*, **7**, 69-89.

Figure 1

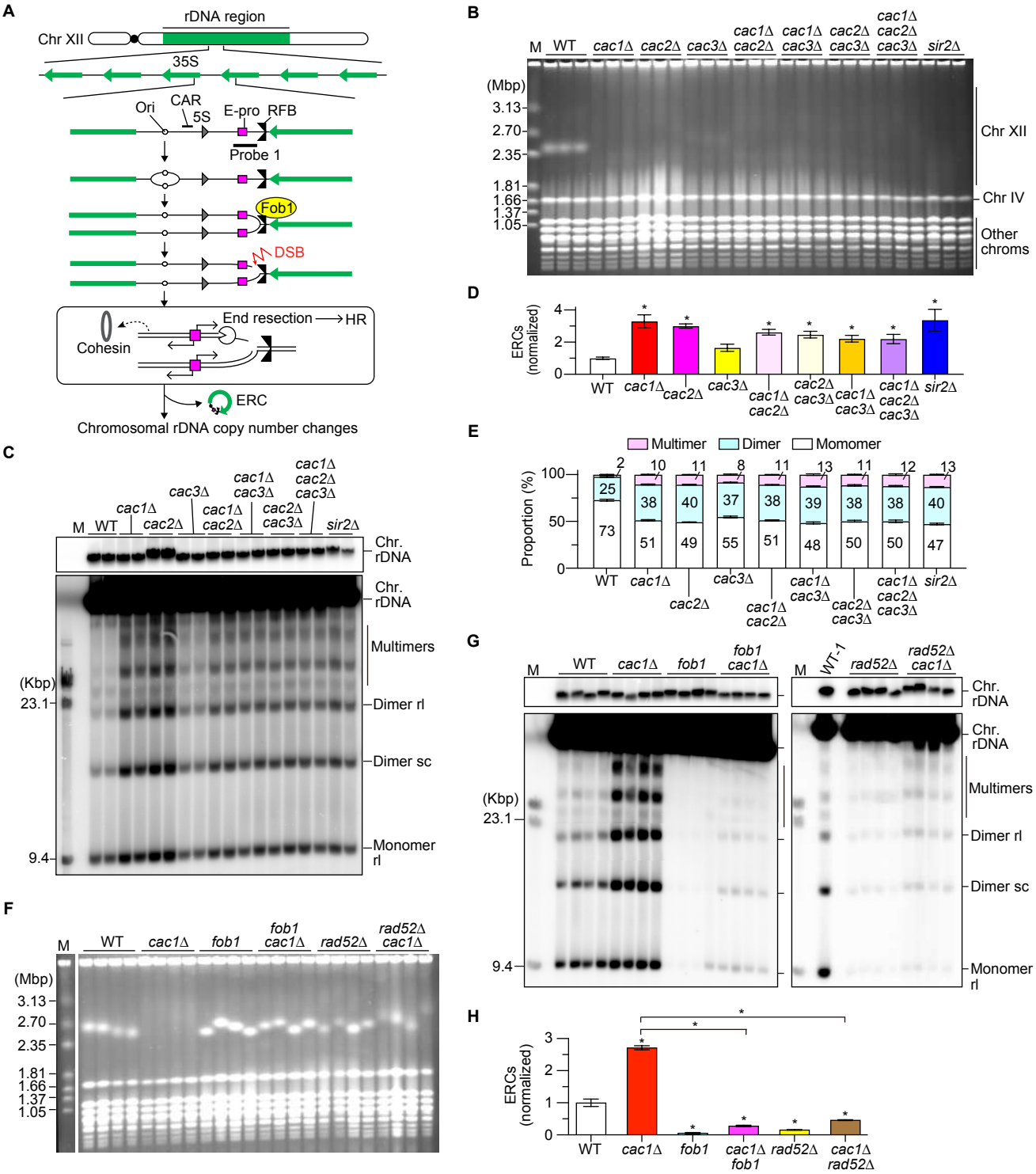

Figure 1. CAF-1 suppresses HR-mediated rDNA instability in response to Fob1-dependent replication fork arrest.
(A) Replication fork arrest, DSB formation, and rDNA copy number changes in the budding yeast rDNA region. Chr XII carries the rDNA cluster, as indicated by the bar, where approximately 150 rDNA copies are tandemly arrayed. Each copy contains 35S rRNA (35S), 5S rRNA (5S), an origin of DNA replication (Ori), a cohesin-associated region (CAR), a bidirectional promoter for noncoding RNA, called E-pro, and a replication fork barrier (RFB). Probe 1 was used for ERC detection.
(B, F) PFGE analysis of chr XII size heterogeneity. DNA from three independent clones (B) and four independent clones (F) of the indicated strains was separated by PFGE and stained with ethidium bromide (EtBr). M indicates *Hansenula wingei* chromosomal DNA markers.
(C, G) ERC detection. DNA was isolated from two independent clones (C) and four independent clones (G) of the indicated strains and separated by agarose gel electrophoresis, followed by Southern blotting with the probe 1, as shown in (A). In (G), DNA from the first WT clone (WT-1) run on the left gel was also loaded on the right gel. Chromosomal rDNA and different ERC forms are indicated. rl and sc indicate relaxed and supercoiled forms of ERCs, respectively. Supercoiled monomers ran off from the gel in the electrophoresis condition used in this experiment. M indicates lambda Hind III DNA markers. The top panel shows short exposure of genomic rDNA signals.
(D, H) Quantitation of ERCs. ERCs from (C) and Supplementary Figure 1A were quantified in (D). ERCs from (G) were quantified in (H). ERC levels were compared between WT and mutants by one-way ANOVA, followed by Tukey's multiple comparisons test. Bars show the mean ± s.e.m. Asterisks indicate statistically significant differences between WT and mutant strains ($p < 0.05$).
(E) Proportion of different ERC forms. In each sample, monomeric, dimeric and multimeric ERCs were quantified and the proportion of each form in total was expressed as proportion of total ERCs.

Figure 2

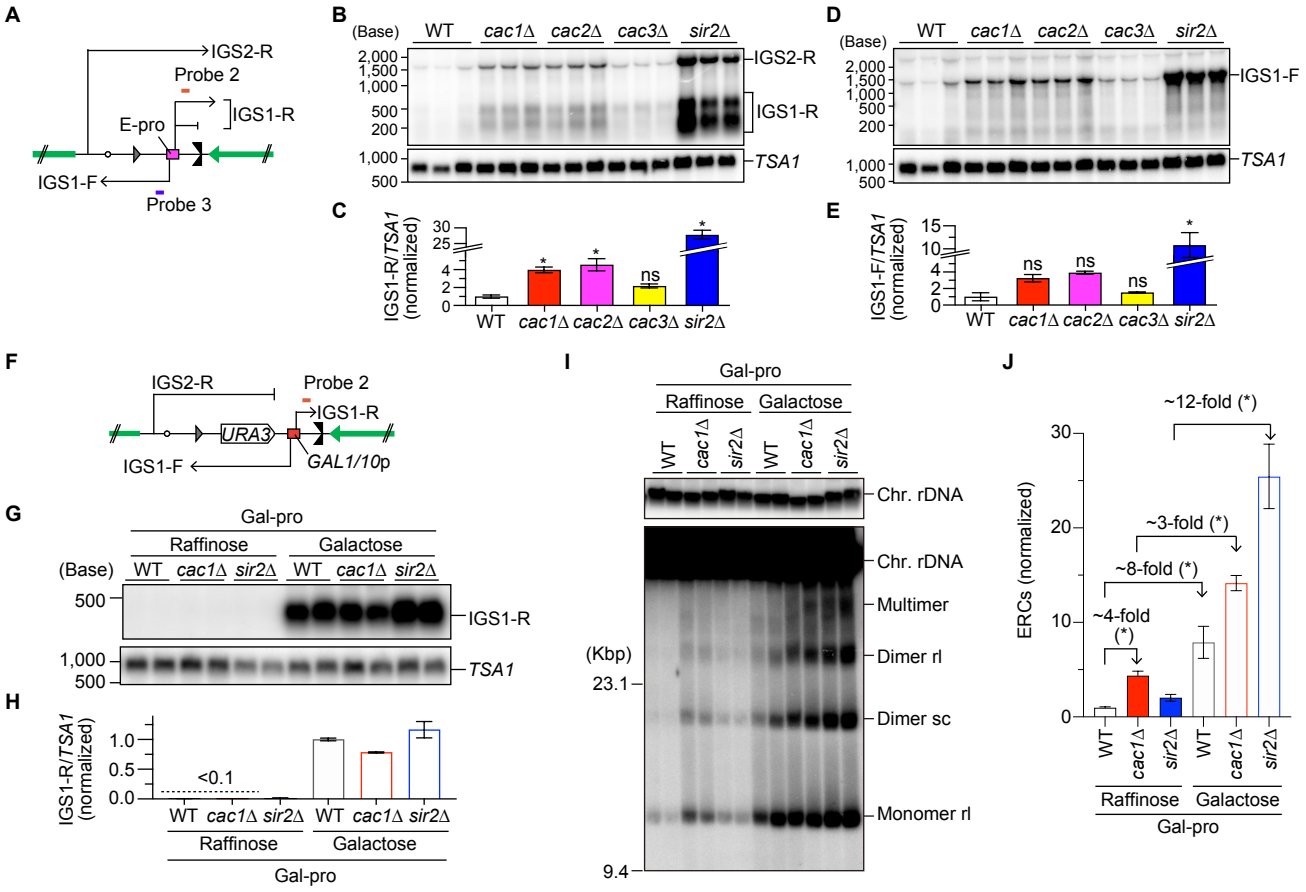

Figure 2. CAF-1 stabilizes the rDNA through both E-pro transcription-dependent and -independent mechanisms.
(A, F) Positions of probes 2 and 3 used for the detection of noncoding RNA by Northern blotting in strains carrying the native E-pro (A) or Gal-pro (F).
(B, D, G) Northern blot analysis of noncoding RNAs transcribed from the intergenic regions in the rDNA. Total RNA was isolated from three independent clones of strains carrying E-pro (B, D) and two independent clones of Gal-pro strains grown in the presence of either raffinose or galactose in the media (G). RNA was separated by size on formaldehyde-agarose gels, followed by Northern blotting. In (B) and (G), IGS1-R transcripts were detected with probe 2. In (D), IGS1-F transcripts were detected with probe 3. The membranes were reprobed for *TSA1* transcripts as a control for loading.
(C, E, H) Quantitation of noncoding RNA. In (C) and (E), signals corresponding to IGS1-R transcripts in (B) and IGS1-F transcripts in (D) were quantified relative to TSA1, respectively, which were normalized to the average of WT clones. In (H), IGS1-F transcripts were normalized to TSA1 and expressed relative to the average of Gal-pro WT clones grown in the presence of galactose. Bars show the mean ± s.e.m. (C, E) and the mean and the range from two independent experiments (H). Transcript levels were compared by one-way ANOVA, followed by Tukey's multiple comparisons test (C, E); *, statistically significant difference between WT and mutants ($p < 0.05$); ns, no significant difference ($p > 0.05$).
(I) ERC detection. DNA was isolated from independent clones of the indicated strains in the Gal-pro background and separated by agarose gel electrophoresis, followed by Southern blotting with the probe 1, as shown in Figure 1A. Chromosomal rDNA and different forms of ERCs are indicated. rl and sc indicate relaxed and supercoiled ERCs, respectively. Supercoiled monomers ran off from the gel in the electrophoresis condition under these conditions. The sizes of lambda Hind III DNA markers are indicated. The top panel shows a short exposure of chromosomal rDNA signals.
(J) Quantitation of ERCs. ERCs were quantified from three independent clones of the indicated strains, including two clones in (H) and a third clone analyzed on a separate gel. ERC levels were compared by the two-sided Student's t-tests. Bars show the mean ± s.e.m. Asterisks above brackets indicate statistically significant differences between strains that were grown in the indicated growth conditions ($p < 0.05$).

Figure 3

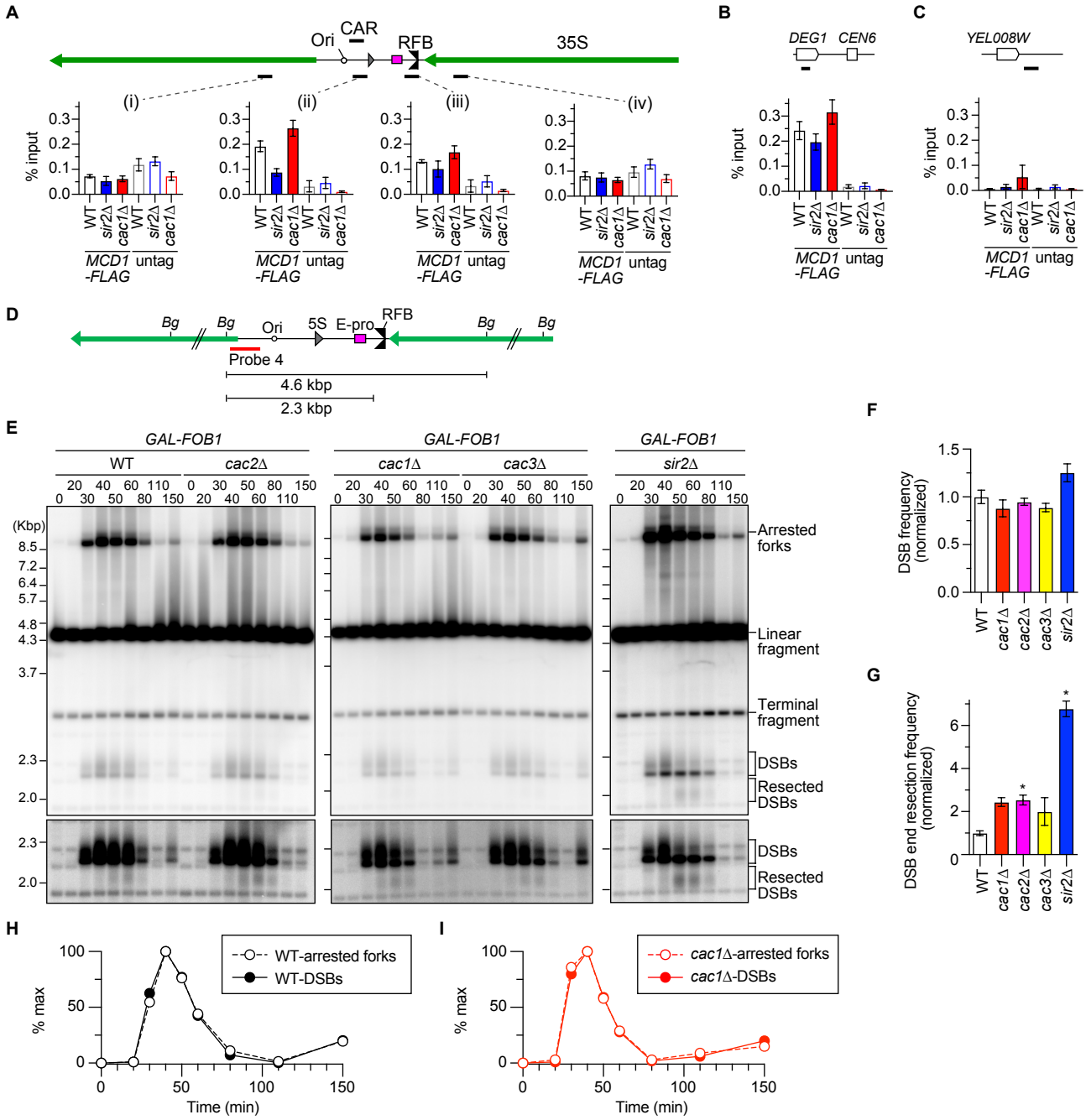

Figure 3. CAF-1 suppresses DSB end resection.

(A, B, C) ChIP–qPCR analyses of Mcd1-Flag in the indicated strains. The regions where cohesin enrichments were examined are indicated as black bars. Four different regions in the rDNA region (i)–(iv) in (A), the positive control region near CEN6 in (B) and the negative control region near YEL088W on chr V (C) were examined. Untagged strains were used as controls. ChIP was performed using an antibody against a Flag epitope tag. The enrichment of chromatin in the indicated regions is expressed as the % input (IP/whole-cell extract). The bars show the mean ± s.e.m. from three independent cultures of each strain.

(D) Restriction map and the positions of the probe 4 used for DSB analyses. The restriction sites for Bgl II (Bg) are indicated.

(E) DSB assay. Time-course experiments were conducted by arresting the indicated strains in the GAL-FOB1 background in G1 with alpha factor, releasing cells into fresh media and collecting cells at different time points, as described in Supplementary Figure S2A. Genomic DNA was isolated, digested with Bgl II, separated by size, and analyzed by Southern blotting with probe 4, as shown in (D). Arrested forks, linear fragments, DSBs and resected DSBs are indicated. Terminal fragments indicate the telomere-proximal rDNA repeat. Long exposure panels around DSBs and resected DSBs are shown below.

(F) Quantitation of DSBs. The frequency of DSBs was determined by quantifying the maximum signal of DSBs relative to the maximum signal of arrested forks in each time course. The average DSB frequency from three independent time course experiments was determined and normalized to the average of WT clones (bars show the mean ± s.e.m.). Multiple comparisons were performed by one-way ANOVA, followed by Tukey's multiple comparisons test. The difference in DSB frequencies between WT and all other mutants was not statistically significant.

(G) Quantitation of resected DSBs. The frequency of resected DSB was determined by quantifying the maximum signal of resected DSBs relative to the maximum signal of DSBs in each time course. The average frequency of resected DSBs from three independent time course experiments was determined and normalized to the average of WT clones (bars show the mean ± s.e.m.). Multiple comparisons were performed by one-way ANOVA, followed by Tukey's multiple comparisons test; *, statistically significant difference ($p < 0.05$).

(H, I) Timing of appearance and disappearance of arrested forks and DSBs. Arrested forks and DSBs are expressed as percent of maximum values in one of the three independent time course experiments of GAL-FOB1 WT (H) and cac1Δ strains (I).

Figure 4

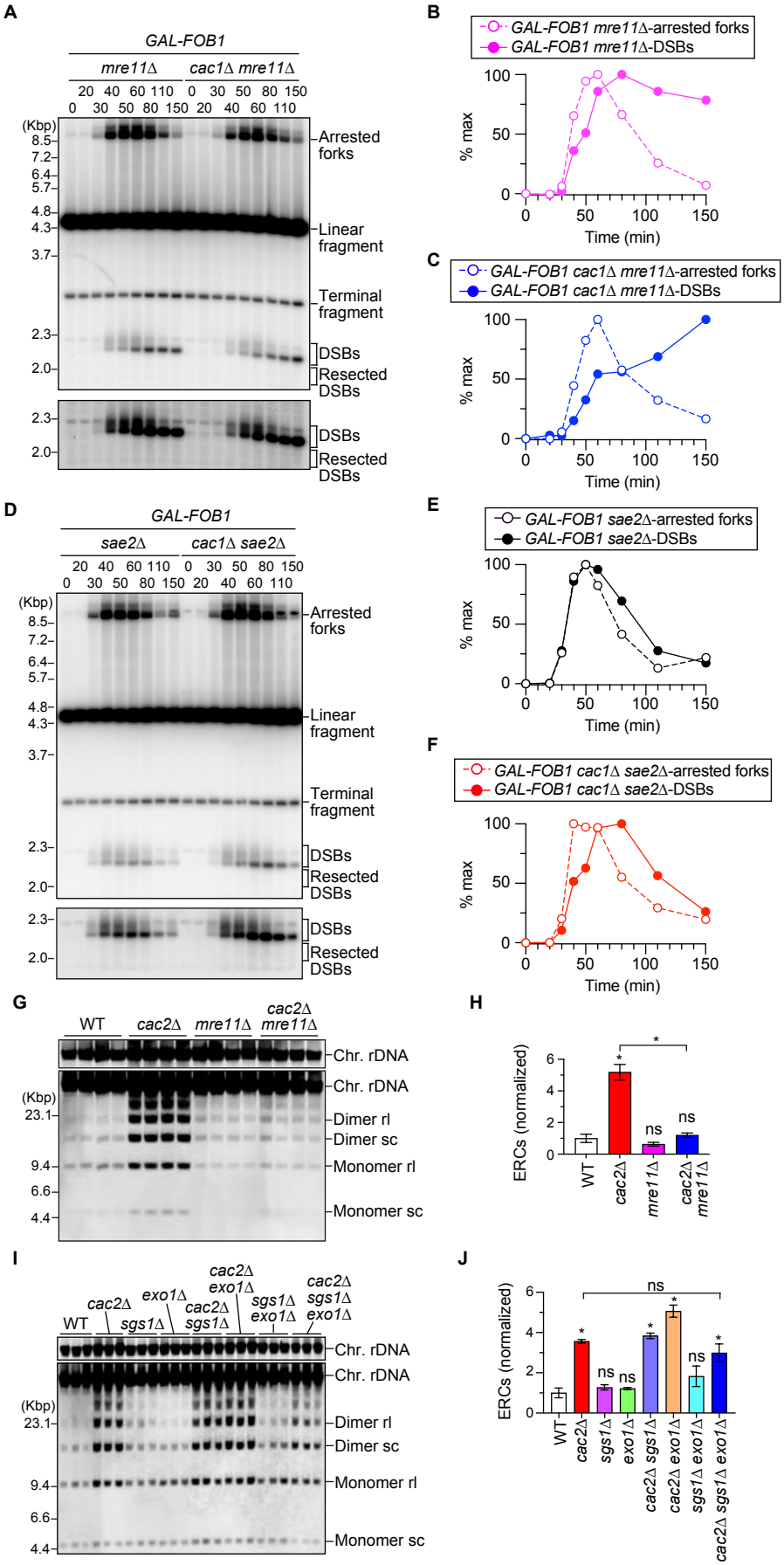

Figure 4. The MRX complex is required for DSB repair and ERC production in the caf-1 mutant.
(A, D) DSB assay. Time-course experiments were conducted by arresting the indicated strains in the GAL-FOB1 background in G1 with alpha factor, releasing cells into fresh media and collecting cells at different time points, as described in Supplementary Figure S2A. Genomic DNA was isolated, digested with Bgl II, separated by size, and analyzed by Southern blotting with probe 4, as shown in Figure 3D. Arrested forks, linear fragments, DSBs, and resected DSBs are indicated. Terminal fragments indicate the telomere-proximal rDNA repeat. Long exposure panels around DSBs and resected DSBs are shown below.
(B, C, E, F) Timing of appearance and disappearance of arrested forks and DSBs. Arrested forks and DSBs are expressed as percent of maximum values in one of the two independent time course experiments of the indicated strains.
(G, **I**) ERC detection. DNA was isolated from four independent clones (H) and three independent clones (K) of the indicated strains and separated by agarose gel electrophoresis, followed by Southern blotting with the probe 1, as shown in Figure 1A. Chromosomal rDNA and different forms of ERCs are indicated. rl and sc indicate relaxed and supercoiled ERCs, respectively. Supercoiled monomers ran off from the gel in the electrophoresis condition under these conditions. The sizes of lambda Hind III DNA markers are indicated. The top panel shows a short exposure of chromosomal rDNA signals.
(H, **J**) Quantitation of ERCs. In (I) and (L), ERCs were quantified from (H) and (K), respectively. ERC levels were compared between WT and mutants by one-way ANOVA, followed by Tukey's multiple comparisons test. Bars show the mean ± s.e.m. Asterisks indicate statistically significant differences between WT and mutant strains ($p < 0.05$). ns indicates no significant difference ($p > 0.05$).

Figure 5

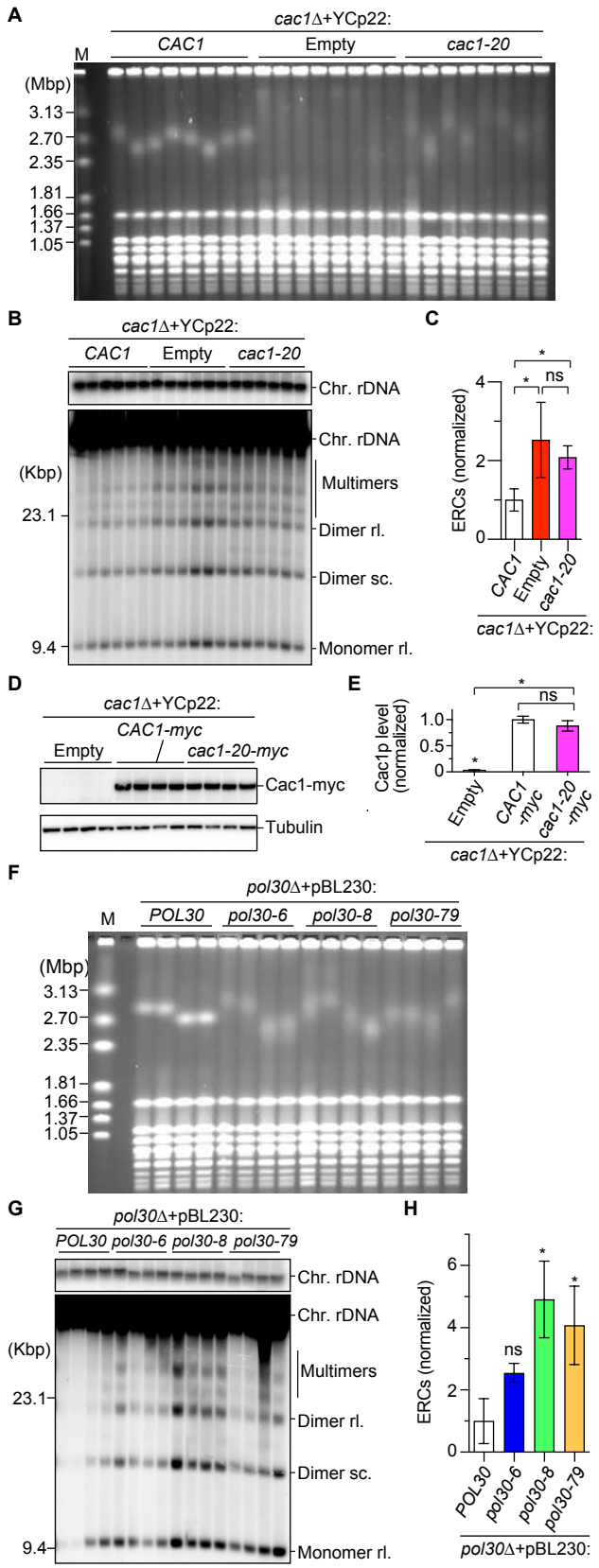

Figure 5. Interaction with PCNA is important for CAF-1 to stabilize the rDNA.

(A, F) PFGE analysis to examine the size heterogeneity of chr XII. DNA from independent clones of the indicated strains was separated by PFGE and stained with EtBr. M indicates *H. wingei* chromosomal DNA markers.

(B, E) ERC detection. DNA was isolated from 6 independent clones (B) and four independent clones (E) of the indicated strains and separated by agarose gel electrophoresis, followed by Southern blotting with the probe 1, as shown in Figure 1A. Genomic rDNA and different forms of ERCs are indicated. M indicates lambda Hind III DNA markers. The top panel shows a short exposure of genomic rDNA signals.

(C, H) Quantitation of ERC levels. ERCs in (B, G) were quantified and their levels were normalized to those of the cac1Δ strain complemented with a plasmid carrying CAC1 in (C) and the pol30Δ strain complemented with a plasmid carrying POL30 in (H). ERC levels among different strains were compared by one-way ANOVA, followed by Tukey's multiple comparisons test. Bars show the mean ± s.e.m. Asterisks above bars and above brackets indicate statistically significant differences between WT and mutant strains and between mutant strains, respectively ($p < 0.05$). ns indicates no significant difference ($p > 0.05$).

(D) Western blot of Cac1 that is C-terminally tagged with a nine Myc epitope and tubulin from four independent clones of the cac1Δ strains that were transformed with a YCp22 vector or the vectors expressing either Cac1-9myc or Cac1-20-9myc.

(E) Quantitation of Cac1-myc protein levels. The levels of Cac1-9myc and Cac1-20-9myc were quantified in the indicated strains relative to tubulin, which was normalized to the average of the *cac1*Δ clones expressing Cac1-9myc. Bars show the mean ± s.e.m. Multiple comparisons were performed by one-way ANOVA, followed by Tukey's multiple comparisons test; *, statistically significant difference ($p < 0.05$); ns, no significant difference ($p > 0.05$).

Figure 6

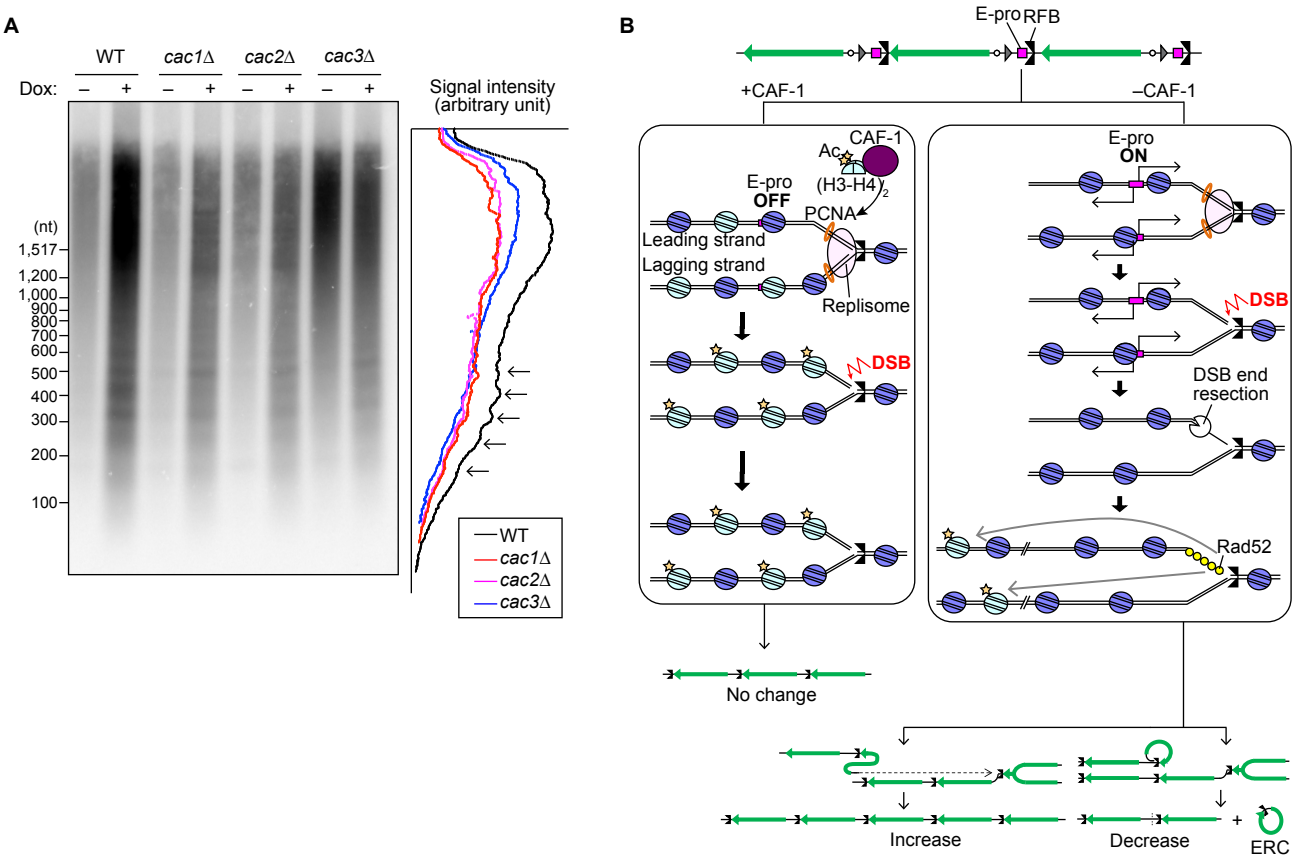

Figure 6. A model for CAF-1-mediated rDNA stabilization.
(A) The size of Okazaki fragments generated during rDNA replication. WT, *cac1*Δ, *cac2*Δ,and *cac3*Δ cells carrying a doxycycline-repressible allele of *CDC9* were treated or not treated with doxycycline (Dox). Genomic DNA was isolated and separated on a denaturing agarose gel, followed by Southern blotting with a rDNA probe 1, as indicated in Figure 1A. Lane profiles of the indicated strains, in which CDC9 was shut off, were included. The positions of the bands of Okazaki fragments are indicated by arrowheads.
(B) A model for CAF-1-mediated rDNA stabilization. Left: CAF-1 facilitates nucleosome assembly onto replicating DNA by depositing a newly synthesized (H3-H4)2 tetramer where H3K56 is acetylated (Ac). The assembly of the properly spaced nucleosome leads to the repression of transcription from E-pro. DSBs formed in this chromatin environment are repaired in a manner that does not involve rDNA copy number changes. Right: The absence of CAF-1 leads to defects in depositing newly synthesized histones. This environment results in the activation of transcription from E-pro, leading to the induction of DSB end resection and HR-mediated DSB repair. The HR protein Rad52 bound to resected DSBs preferentially uses the rDNA copy in a chromatin environment with histone H3K56Ac. Because the density of histone H3 acetylated at K56 is low in the CAF-1-defective strain, Rad52 assembled on the replicated DNA preferentially uses the distant rDNA copy, inducing rDNA instability. This template choice error may not be affected by transcription at the E-pro.